

Lawrence Berkeley National Laboratory

LBL Publications

Title

Measurement of the CKM angle γ in the $B_0 \rightarrow DK^*0$ channel using self-conjugate $D \rightarrow KS_0 h^+ h^-$ decays

Permalink

<https://escholarship.org/uc/item/8bv1m9xh>

Journal

European Physical Journal C, 84(2)

ISSN

1434-6044

Authors

Aaij, R
Abdelmotteleb, ASW
Beteta, C Abellan
[et al.](#)

Publication Date

2024

DOI

10.1140/epjc/s10052-023-12376-z

Copyright Information

This work is made available under the terms of a Creative Commons Attribution License, available at <https://creativecommons.org/licenses/by/4.0/>

Peer reviewed



Measurement of the CKM angle γ in the $B^0 \rightarrow DK^{*0}$ channel using self-conjugate $D \rightarrow K_S^0 h^+ h^-$ decays

LHCb collaboration*

CERN, 1211 Geneva 23, Switzerland

Received: 20 October 2023 / Accepted: 20 December 2023 / Published online: 29 February 2024
© CERN for the benefit of The LHCb Collaboration 2024

Abstract A model-independent study of CP violation in $B^0 \rightarrow DK^{*0}$ decays is presented using data corresponding to an integrated luminosity of 9fb^{-1} collected by the LHCb experiment at centre-of-mass energies of $\sqrt{s} = 7, 8$ and 13TeV . The CKM angle γ is determined by examining the distributions of signal decays in phase-space bins of the self-conjugate $D \rightarrow K_S^0 h^+ h^-$ decays, where $h = \pi, K$. Observables related to CP violation are measured and the angle γ is determined to be $\gamma = (49_{-19}^{+22})^\circ$. Measurements of the amplitude ratio and strong-phase difference between the favoured and suppressed B^0 decays are also presented.

1 Introduction

In the Standard Model (SM), the Cabibbo–Kobayashi–Maskawa (CKM) matrix [1,2] describes flavour-changing weak transitions of quarks. The phase difference between the CKM matrix elements for $b \rightarrow u$ and $b \rightarrow c$ quark transitions, defined as $\gamma \equiv \arg(-V_{ud}V_{ub}^*/V_{cd}V_{cb}^*)$, is of particular interest because it is measurable in purely tree-level decays and has negligible theoretical uncertainty [3]. Therefore, the SM can be tested by comparing direct measurements of γ with indirect determinations obtained by fitting the CKM unitarity triangle. The average value of the direct measurements is $\gamma_{\text{direct}} = (66.2_{-3.6}^{+3.4})^\circ$ [4], which agrees at current precision with the indirectly determined value $\gamma_{\text{indirect}} = (65.6_{-2.7}^{+0.9})^\circ$ [5] or $\gamma_{\text{indirect}} = (65.8 \pm 2.2)^\circ$ [6] depending on the statistical approach used. A more stringent test requires improving the precision on both the direct and indirect determinations of γ .

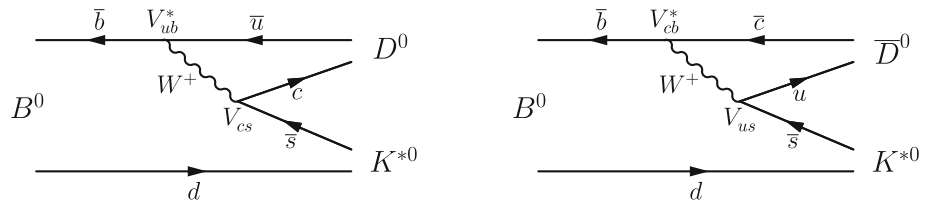
The precision on γ is dominated by the measured CP violation in the interference between $b \rightarrow u\bar{c}s$ and $b \rightarrow c\bar{u}s$ quark transitions in $B^\pm \rightarrow DK^\pm$ decays. Here, D represents a superposition of D^0 and \bar{D}^0 mesons. However it is possible to gain complementary information from the $B^0 \rightarrow DK^*(892)^0$ decay.¹ While this decay has a lower branching fraction compared to the $B^\pm \rightarrow DK^\pm$ channel, the interference between the favoured and suppressed $B^0 \rightarrow DK^{*0}$ decays is expected to be a factor of 3 larger since both amplitudes are colour suppressed, leading to a higher per-event sensitivity to γ . Feynman diagrams of the two possible B^0 decays are shown in Fig. 1. The flavour of the B meson at the point of decay is unambiguously provided by the charge of the kaon from the $K^*(892)^0 \rightarrow K^+\pi^-$ decay, and hence the analysis of this channel can proceed without considering time dependence. Interference between the two amplitudes is accessed through reconstruction of the D meson in final states common to both D^0 and \bar{D}^0 . For the analysis presented here the D mesons are reconstructed in the self-conjugate $D \rightarrow K_S^0 h^+ h^-$ decay modes ($h = \pi, K$). The Belle [7,8] and BaBar [9] collaborations have used the $B^0 \rightarrow DK^{*0}$ channel to determine γ with various final states of D decay, including $D \rightarrow K_S^0 \pi^+ \pi^-$. However, the most precise measurements using the $B^0 \rightarrow DK^{*0}$ decay mode have been made by the LHCb experiment [10,11].

The work presented here uses data collected with the LHCb detector in proton-proton (pp) collisions at centre-of-mass energies of $\sqrt{s} = 7, 8$ and 13TeV between 2011–2012 and 2015–2018, corresponding to an integrated luminosity of 9fb^{-1} . The experimental procedure employed here closely follows that described in Ref. [11], where CP violation observables that are related to γ are determined through the distributions of $B^0 \rightarrow DK^{*0}$ and $\bar{B}^0 \rightarrow D\bar{K}^{*0}$ decays in regions of the $D \rightarrow K_S^0 h^+ h^-$ decay phase space [12–15]. The extraction of γ requires knowledge of the D decay strong-phase parameters, which were directly determined by

¹ The inclusion of charge-conjugate processes is implied, unless explicitly stated otherwise.

* e-mail: innes.mackay@physics.ox.ac.uk

Fig. 1 Feynman diagrams for the (left) suppressed and (right) favoured $B^0 \rightarrow DK^{*0}$ decays



the BESIII [16–18] and CLEO [19] collaborations. Therefore, the measurement avoids using any D decay amplitude model, thus is free of any systematic uncertainty attributed to such models.

The data set used for the work presented here is increased compared to Ref. [11]. In addition, a number of procedural improvements are made, such as adopting a more optimal division of $D \rightarrow K_S^0 \pi^+ \pi^-$ phase space, and employing an improved strategy to handle the varying reconstruction efficiency over D decay phase space. Furthermore, the strong-phase inputs are updated to reflect the most recent combination of results from CLEO and BESIII [16, 17].

2 Analysis overview

The amplitudes of the favoured and suppressed $B^0 \rightarrow DK^+ \pi^-$ decays, where the $K^+ \pi^-$ is not restricted to the K^{*0} resonance, can be written as

$$A(B^0 \rightarrow \bar{D}^0 K^+ \pi^-) \equiv A_c(p) e^{i\delta_c(p)} \quad (\text{favoured}), \tag{1}$$

$$A(B^0 \rightarrow D^0 K^+ \pi^-) \equiv A_u(p) e^{i[\delta_u(p)+\gamma]} \quad (\text{suppressed}), \tag{2}$$

where $A_{c(u)}$ and $\delta_{c(u)}$ are the magnitude and strong-phase of the decay corresponding to the $b \rightarrow c(u)$ transitions, respectively, and p is the phase-space coordinate of the $DK^+ \pi^-$ final state. The equivalent amplitudes for the CP conjugate, $\bar{B}^0 \rightarrow DK^- \pi^+$, are given by transforming $\gamma \rightarrow -\gamma$. In this analysis, the amplitude ratio (r_{B^0}) and strong-phase difference (δ_{B^0}) between the favoured and suppressed signal decays are measured alongside the angle γ . They are defined as

$$r_{B^0}^2 = \frac{\int_{K^{*0}} dp A_u(p)^2}{\int_{K^{*0}} dp A_c(p)^2}, \tag{3}$$

$$\kappa e^{i\delta_{B^0}} = \frac{\int_{K^{*0}} dp A_c(p) A_u(p) e^{i[\delta_u(p)-\delta_c(p)]}}{\sqrt{\int_{K^{*0}} dp A_c(p)^2} \sqrt{\int_{K^{*0}} dp A_u(p)^2}}, \tag{4}$$

where the integral is performed over the $B^0 \rightarrow DK^{*0}$ region of the $B^0 \rightarrow DK^+ \pi^-$ phase space. The coherence factor, κ , accounts for pollution from decays that are not $B^0 \rightarrow DK^{*0}$, and satisfies $0 \leq \kappa \leq 1$. The value of $\kappa = 0.958^{+0.005}_{-0.046}$ is used as a direct input from the LHCb amplitude analysis of

$B^0 \rightarrow DK^+ \pi^-$ decays described in Ref. [20]. The kinematic selection of the K^{*0} candidates used in this work follows that of Ref. [20] to match the phase-space region in which κ is evaluated.

The amplitudes for the $D^0 \rightarrow K_S^0 h^+ h^-$ and $\bar{D}^0 \rightarrow K_S^0 h^+ h^-$ decays are written as $A_D(m_-^2, m_+^2) = |A_D(m_-^2, m_+^2)| e^{i\delta(m_-^2, m_+^2)}$ and $A_{\bar{D}}(m_-^2, m_+^2) = |A_{\bar{D}}(m_-^2, m_+^2)| e^{i\bar{\delta}(m_-^2, m_+^2)}$, respectively, where $m_{\pm}^2 = m^2(K_S^0 h^{\pm})$ are the Dalitz plot coordinates. The D decay phase space is divided into independent regions. A scheme is used with $2\mathcal{N}$ bins labelled from $i = -\mathcal{N}$ to $i = \mathcal{N}$ (excluding 0). The division is symmetrical about the line $m_-^2 = m_+^2$, and a bin where $m_-^2 > m_+^2$ ($m_-^2 < m_+^2$) is referred to as the i^{th} ($-i^{th}$) bin. The ‘optimal’ [19] (‘2-bin’) scheme with $\mathcal{N} = 8$ ($\mathcal{N} = 2$) bins is used for the $D \rightarrow K_S^0 \pi^+ \pi^-$ ($D \rightarrow K_S^0 K^+ K^-$) mode, and is displayed in Fig. 2.

The total amplitude of the $B^0 \rightarrow (K_S^0 h^+ h^-)_D K^+ \pi^-$ decay is given by

$$A(B^0 \rightarrow (K_S^0 h^+ h^-)_D K^+ \pi^-) = A_c(p) e^{i\delta_c(p)} A_{\bar{D}}(m_-^2, m_+^2) + A_u(p) e^{i[\delta_u(p)+\gamma]} A_D(m_-^2, m_+^2), \tag{5}$$

where that of the CP conjugate \bar{B}^0 decay is found by transforming $\gamma \rightarrow -\gamma$ and $m_- \leftrightarrow m_+$. Squaring the total amplitude and integrating over the K^{*0} phase-space region gives

$$\Gamma(B^0 \rightarrow (K_S^0 h^+ h^-)_D K^{*0}) \propto |A_{\bar{D}}|^2 + r_{B^0}^2 |A_D|^2 + 2\kappa r_{B^0} |A_D| |A_{\bar{D}}| \left[\cos(\delta_{B^0} + \gamma) \cos \delta_D - \sin(\delta_{B^0} + \gamma) \sin \delta_D \right], \tag{6}$$

where the Dalitz plot coordinates of the D decay strong-phase difference, defined as $\delta_D(m_-^2, m_+^2) = \delta(m_-^2, m_+^2) - \bar{\delta}(m_-^2, m_+^2)$, and magnitudes have been omitted for brevity. The expression for the decay rate integrated over a Dalitz plot bin is given by

$$\Gamma_i(B^0 \rightarrow (K_S^0 h^+ h^-)_D K^{*0}) \propto K_{-i} + r_{B^0}^2 K_i + 2\kappa r_{B^0} \sqrt{K_i K_{-i}} [\cos(\delta_{B^0} + \gamma) c_i - \sin(\delta_{B^0} + \gamma) s_i], \tag{7}$$

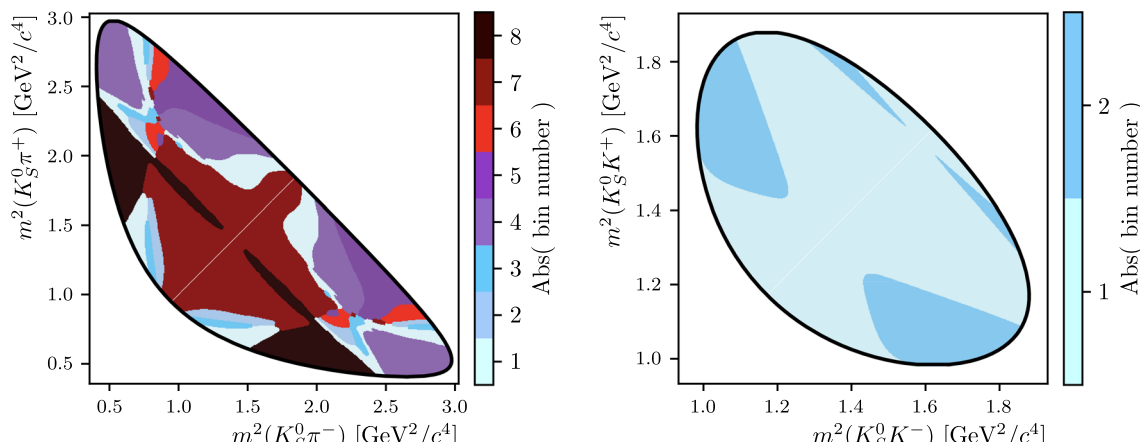


Fig. 2 Dalitz plot binning schemes used for (left) $D \rightarrow K_S^0 \pi^+ \pi^-$ and (right) $D \rightarrow K_S^0 K^+ K^-$ decays

where the D decay magnitude and strong-phase difference have been replaced by integrals over Dalitz plot bins

$$K_i = \int_i dm_-^2 dm_+^2 |A_D(m_-^2, m_+^2)|^2, \tag{8}$$

$$c_i = \frac{1}{\sqrt{K_i K_{-i}}} \times \int_i dm_-^2 dm_+^2 |A_D(m_-^2, m_+^2)| |A_{\bar{D}}(m_-^2, m_+^2)| \cos \delta_D(m_-^2, m_+^2), \tag{9}$$

$$s_i = \frac{1}{\sqrt{K_i K_{-i}}} \times \int_i dm_-^2 dm_+^2 |A_D(m_-^2, m_+^2)| |A_{\bar{D}}(m_-^2, m_+^2)| \sin \delta_D(m_-^2, m_+^2). \tag{10}$$

Swapping the coordinates $m_- \leftrightarrow m_+$ is equivalent to a bin transformation $i \leftrightarrow -i$, and results in the relations $c_i = c_{-i}$ and $s_i = -s_{-i}$.

Experimentally, candidate yields are determined instead of the decay rates. Detector, reconstruction and selection related efficiencies are accounted for by using a set of parameters referred to as F_i that are determined in each bin. They are defined as

$$F_i \equiv \frac{\int_i dm_-^2 dm_+^2 |A_D(m_-^2, m_+^2)|^2 \eta(m_-^2, m_+^2)}{\sum_j \int_j dm_-^2 dm_+^2 |A_D(m_-^2, m_+^2)|^2 \eta(m_-^2, m_+^2)}, \tag{11}$$

where $\eta(m_-^2, m_+^2)$ is the efficiency profile which varies over the D decay phase space. The F_i are the efficiency-modulated K_i parameters, and are dependent on the experimental resolution and selection efficiency. A similar efficiency adjustment is not included in the c_i and s_i parameters because the effect is small, however a systematic uncertainty is included to account for this assumption. The F_i parameters have been determined using $B^\pm \rightarrow D\pi^\pm$ decays [21]. As these parameters are selection dependent, they are only valid for use in this analysis under the assumption that the relative variation

in $\eta(m_-^2, m_+^2)$ between D meson decays in $B^\pm \rightarrow D\pi^\pm$ and $B^0 \rightarrow DK^{*0}$ is the same. Differences in the efficiency profiles are minimised by employing a similar selection between the $B^0 \rightarrow DK^{*0}$ and $B^\pm \rightarrow D\pi^\pm$ decays and small residual differences are determined using simulation samples and used to assign systematic uncertainties on the CP violation observables. The yields of B^0 and \bar{B}^0 decays in a Dalitz plot bin are given by

$$N_i(B^0) = h^{B^0} [F_{-i} + (x_+^2 + y_+^2)F_i + 2\kappa\sqrt{F_i F_{-i}}(x_+c_i - y_+s_i)], \tag{12}$$

$$N_i(\bar{B}^0) = h^{\bar{B}^0} [F_i + (x_-^2 + y_-^2)F_{-i} + 2\kappa\sqrt{F_i F_{-i}}(x_-c_i + y_-s_i)], \tag{13}$$

where the CP violation observables [22], x_\pm and y_\pm , are related to the physics parameters by

$$x_\pm \equiv r_{B^0} \cos(\delta_{B^0} \pm \gamma), \tag{14}$$

$$y_\pm \equiv r_{B^0} \sin(\delta_{B^0} \pm \gamma). \tag{15}$$

These observables have improved statistical behaviour in comparison to determining γ , r_{B^0} and δ_{B^0} directly. The two normalisation constants in Eqs. (12) and (13), h^{B^0} and $h^{\bar{B}^0}$, are the observed total yields of the B^0 and \bar{B}^0 decay modes. The use of two separate normalization constants is intentional, as nearly all detector and production asymmetries are absorbed into these parameters leaving the measurement insensitive to these effects. Equations (12) and (13) are used to fit the data and determine the CP violation observables. In the fit, the external input parameters κ [20], F_i [21], c_i and s_i [16, 17] are fixed to their measured central values.

The $\bar{B}_s^0 \rightarrow D^0 K^{*0}$ decay, which has identical final state particles is reconstructed alongside the signal channel. In principle, the method described in this section could also be applied to $\bar{B}_s^0 \rightarrow DK^{*0}$ decays. However, the sensitivity to γ is significantly lower due to reduced interference between the

two final state paths. The values of the CKM elements [23] can be used to predict that the ratio of suppressed to favoured amplitudes, $r_{B_s^0} \sim 0.02$, is over a factor of 10 less than in $B^0 \rightarrow DK^{*0}$ decays [24]. In this analysis it is assumed that the CP violation in the $\bar{B}_s^0 \rightarrow DK^{*0}$ decay is zero and it is not treated as a signal decay mode. Thus in the remainder of the paper this decay is referred to as the $\bar{B}_s^0 \rightarrow D^0 K^{*0}$ background with a flavour specific D meson.

3 Detector and simulation

The LHCb detector [25,26] is a single-arm forward spectrometer covering the pseudorapidity range $2 < \eta < 5$, designed for the study of particles containing b or c quarks. The detector includes a high-precision tracking system consisting of a silicon-strip vertex detector surrounding the pp interaction region, a large-area silicon-strip detector located upstream of a dipole magnet with a bending power of about 4 Tm, and three stations of silicon-strip detectors and straw drift tubes placed downstream of the magnet. The tracking system provides a measurement of the momentum, p , of charged particles with a relative uncertainty that varies from 0.5% at low momentum to 1.0% at 200 GeV/c. The minimum distance of a track to a primary pp collision vertex (PV), the impact parameter (IP), is measured with a resolution of $(15 + 29/p_T) \mu\text{m}$, where p_T is the component of the momentum transverse to the beam, in GeV/c. Different types of charged hadrons are distinguished using information from two ring-imaging Cherenkov detectors. Photons, electrons and hadrons are identified by a calorimeter system consisting of scintillating-pad and preshower detectors, an electromagnetic and a hadronic calorimeter. Muons are identified by a system composed of alternating layers of iron and multiwire proportional chambers.

The online event selection is performed by a trigger, which consists of a hardware stage, based on information from the calorimeter and muon systems, followed by a software stage, which applies a full event reconstruction. The events that are selected for the analysis either have final-state tracks of the signal decay that are subsequently associated with an energy deposit in the calorimeter system that satisfies the hardware stage trigger, or are selected because one of the other particles in the event, not reconstructed as part of the signal candidate, fulfills any hardware stage trigger requirement. At the software stage, it is required that at least one particle should have high p_T and high χ_{IP}^2 , where χ_{IP}^2 is defined as the difference in the primary vertex fit χ^2 with and without the inclusion of that particle. A multivariate algorithm [27] is used to select secondary vertices consistent with being a two-, three-, or four-track b-hadron decay.

Simulated data are required to determine the invariant-mass shapes of signal and background components, and to compute relative selection efficiencies. In the simulation, pp collisions are generated using PYTHIA [28,29] with a specific LHCb configuration [30]. Decays of unstable particles are described by EVTGEN [31], in which final-state radiation is generated using PHOTOS [32]. The decays $D \rightarrow K_S^0 \pi^+ \pi^-$ and $D \rightarrow K_S^0 K^+ K^-$ are generated uniformly over phase space. The interaction of the generated particles with the detector, and its response, are implemented using the GEANT4 toolkit [33,34] as described in Ref. [35].

4 Candidate selection

All tracks and decay vertices are required to be of good quality, and the reconstructed mass of the K_S^0 , D and K^{*0} candidates must be close to their known values [23]. The K_S^0 candidates are formed from two oppositely charged pions, where the tracks are reconstructed using hits in the vertex detector and other downstream tracking stations, or only the latter. These track types are referred to as *long* and *downstream*, respectively, and are treated separately since the former leads to better mass, momentum and vertex resolution on the K_S^0 candidate and higher reconstruction efficiency. A D meson candidate is formed by combining a K_S^0 candidate with two oppositely charged pions. Particle identification (PID) requirements are placed on the particles, to reduce background from $D \rightarrow K_S^0 K^+ \pi^-$ decays, semileptonic D decays, and hadronic decays in flight to leptons. A requirement is placed on the displacement of the D meson vertex from the B meson vertex to reduce background from B decays to the final state particles without the intermediate D meson. The D meson candidate is then combined with a K^{*0} candidate, which is formed by combining a pion and kaon, with strict PID requirements to suppress $B^0 \rightarrow D\pi^+\pi^-$ backgrounds and thus allow for correct identification of the B -meson flavour. A criterion is applied on the K^{*0} helicity angle, θ^* , defined as the angle between the kaon from the K^{*0} decay and the opposite of the B momentum in the K^{*0} rest frame, to exploit differences in the angular distributions of the signal and background candidates. In signal decays, a B meson decays to a vector and pseudo-scalar final state, so the corresponding distribution of $|\cos \theta^*|$ peaks at 1, whereas it is flat for background candidates formed from random combinations of tracks, referred to as combinatorial background. Therefore, candidates are rejected if the value of $|\cos \theta^*|$ is below a threshold that is chosen to match that applied in Ref. [20].

A kinematic fit is performed to improve the resolution of the invariant-mass of the B^0 candidates and Dalitz plot coordinates. In this fit, the masses of the D and K_S^0 candidates are constrained to their known values [23], and the momentum

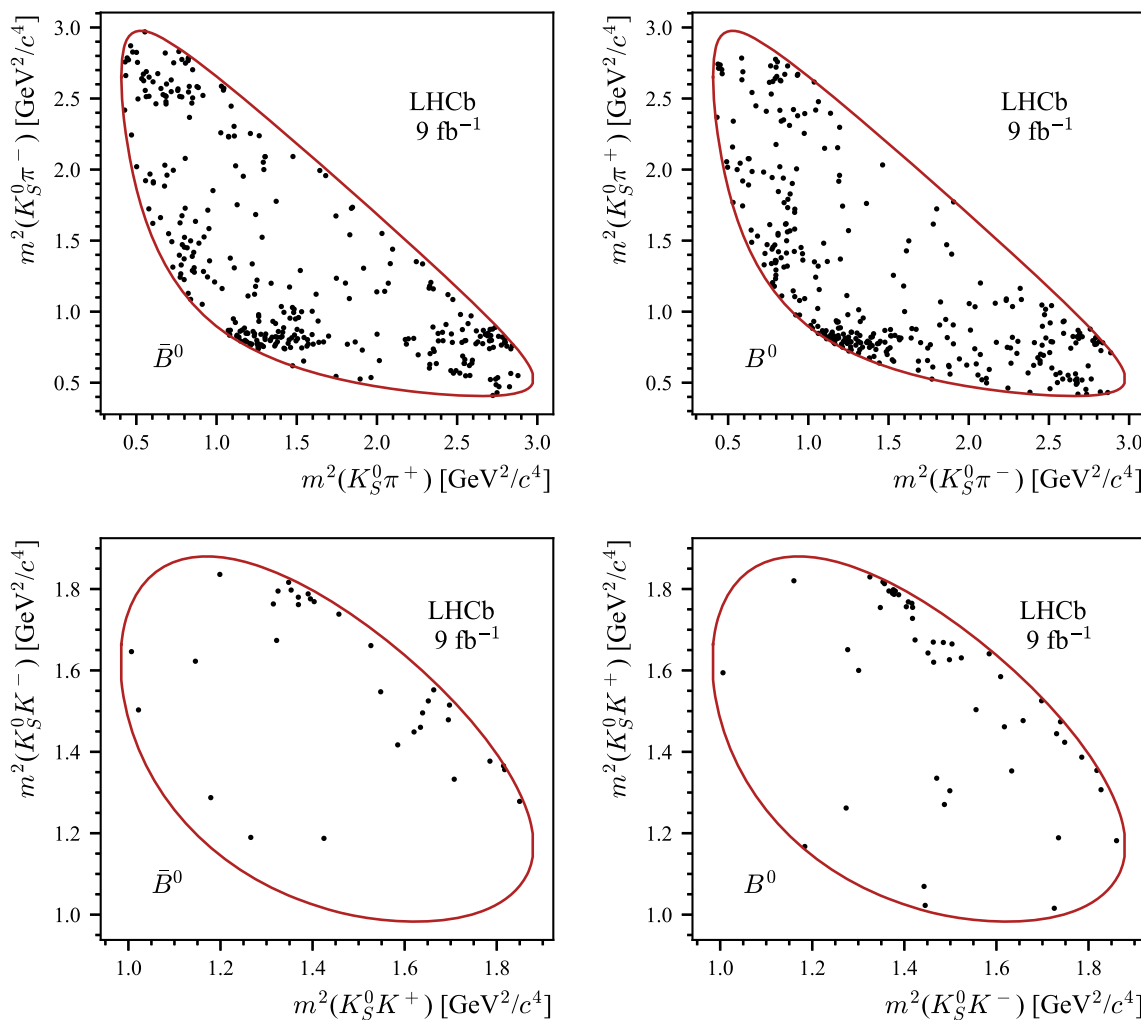


Fig. 3 Dalitz plots of selected candidates for (left) \bar{B}^0 and (right) B^0 decays followed by the (upper) $D \rightarrow K_S^0 \pi^+ \pi^-$ and (lower) $D \rightarrow K_S^0 K^+ K^-$ decay. Candidates that have an invariant mass within

a $30 \text{ MeV}/c^2$ region either side of the B^0 mass are displayed. The kinematic boundaries are plotted as continuous red solid curves

of the B^0 meson is required to be parallel to the vector linking the B^0 decay vertex and the associated PV, which is defined as the PV leading to the smallest IP of the B^0 candidate.

A boosted decision tree (BDT) classifier [36,37] is employed to reduce combinatorial background. It is trained on $B^0 \rightarrow DK^{*0}$ decays with $D \rightarrow K_S^0 \pi^+ \pi^-$ separately for candidates with *long* and *downstream* K_S^0 track types, and is applied to both D decay modes. Signal is represented by simulated decays, and combinatorial background is represented by $B^0 \rightarrow DK^{*0}$ candidates in data with an invariant mass between 5800 and $6200 \text{ MeV}/c^2$. The set of input variables are predominantly based on the decay topology and kinematics. They are taken from the BDT classifier applied in the analysis of $B^\pm \rightarrow Dh^\pm$ decays outlined in Ref. [21]. Since there is an extra track in $B^0 \rightarrow DK^{*0}$ decays, the p , p_T and χ_{IP}^2 of the pion from the K^{*0} decay are also included.

The optimal BDT classifier selection criterion is chosen to minimise the statistical uncertainty on γ and is determined with pseudoexperiments.

Figure 3 displays Dalitz plot distributions of fully selected $B^0 \rightarrow DK^{*0}$ candidates that have an invariant mass within $\pm 30 \text{ MeV}/c^2$ of the B^0 mass [23], where the signal purity is approximately 60%. They are displayed in four categories given by the D decay and B -meson flavour, and candidates from both K_S^0 track types are combined for visualisation purposes only.

5 Fit to determine the CP violation observables

A two-stage fit strategy is adopted to determine the CP violation observables. The same model is used for both stages

in an unbinned maximum likelihood fit to the invariant-mass distribution of $B^0 \rightarrow DK^{*0}$ candidates in the region $5200\text{--}5800\text{ MeV}/c^2$. The lower end of the fit range is chosen to remove background from CP violating $B^0 \rightarrow D^*K^*$ decays. The first stage, referred to as the global fit, is used to understand the background composition and parameterize the invariant-mass distribution. The candidates in this fit are divided into four groups, given by the D decay mode and the K_S^0 track type. In the second stage the data are simultaneously fitted across 80 categories given by the D decay mode, K_S^0 track type, B -meson flavour and Dalitz plot bin.

Due to the similarities in the final state, the signal and $\bar{B}_s^0 \rightarrow D^0K^{*0}$ decays have a similar invariant mass shape. Both are modelled by a function with a Gaussian core and asymmetric tails,

$$f(m) = \begin{cases} \exp(-\delta m^2 (\frac{1+\beta\delta m^2}{f_L})), & \delta m < 0 \\ \exp(-\delta m^2 (\frac{1+\beta\delta m^2}{f_R})), & \delta m > 0 \end{cases} \quad \text{where} \quad \begin{aligned} \delta m &= m - \mu, \\ f_L &= 2\sigma_L^2 + \alpha_L \delta m^2, \\ f_R &= 2(\frac{\sigma_L}{r})^2 + \alpha_R \delta m^2 \end{aligned} \quad (16)$$

where μ is the mean, β is the asymmetry, $\sigma_{L,R}$ and $\alpha_{L,R}$ describe the left and right widths and tails, respectively. The β , α and width ratio, $r = \frac{\sigma_L}{\sigma_R}$, parameters are fixed to values determined from simulation. The mean of the distribution representing $\bar{B}_s^0 \rightarrow D^0K^{*0}$ candidates is a free parameter shared between the categories, whilst that of signal is constrained using the known mass difference, $m(B_s^0) - m(B^0) = (87.42 \pm 0.16)\text{ MeV}/c^2$ [23]. Finally, the width is shared between signal and $\bar{B}_s^0 \rightarrow D^0K^{*0}$ decays for both D decay modes but different for *long* and *downstream* K_S^0 track categories.

The dominant physics background near the signal is from $\bar{B}_s^0 \rightarrow D^{*0}K^{*0}$ candidates with the D^{*0} decaying to a D^0 and an unreconstructed γ or π^0 . The mass model of this background is described by four components depending on which particle is missed and whether the helicity state of the D^{*0} is 0 or ± 1 (the distributions of the ± 1 states are indistinguishable). The parameters describing the shape of each component are fixed to the values determined in simulation. It is not possible to determine the relative fractions of these four components reliably using data collected with the self-conjugate $D \rightarrow K_S^0 h^+ h^-$ modes, because the invariant-mass region below $5200\text{ MeV}/c^2$ is dominated by a mix of $B^0 \rightarrow D^*K^{*0}$ and $\bar{B}_s^0 \rightarrow D^{*0}K^{*0}$ decays and their distributions significantly overlap. However, in Cabibbo-favoured D meson decays the low invariant-mass region is dominated by either \bar{B}_s^0 or B^0 decays. This advantage is used by fitting the invariant mass distribution of candidates reconstructed as $\bar{B}_s^0 \rightarrow D^0(\rightarrow K^-\pi^+)K^{*0}$ decays to determine the relative fractions of each partially reconstructed $\bar{B}_s^0 \rightarrow D^{*0}K^{*0}$ component. The selection of candidates and the mass fit parameterisation follows that described in Ref.

[10], but the data set is increased to include that collected in 2017 and 2018. Given the studies in Ref. [38], contamination from $\bar{B}_s^0 \rightarrow D^{*0}K\pi$ decays that do not include the K^{*0} resonance is small and this background will be subsumed into either the $\bar{B}_s^0 \rightarrow D^{*0}K^{*0}$ shapes or the combinatorial background. A small amount of $B^0 \rightarrow D^*K^{*0}$ decays leaks into the fit range. Their invariant-mass shape and yield ratio are determined in a similar way to that for the $\bar{B}_s^0 \rightarrow D^{*0}K^{*0}$ background by studying candidates reconstructed as $B^0 \rightarrow D(\rightarrow K\pi)K^{*0}$.

Backgrounds from $B^\pm \rightarrow DK^\pm$ decays plus a random pion, and misidentified $B^0 \rightarrow D\pi^+\pi^-$ decays are represented by shapes determined using simulation samples. The relative yield of both are fixed with respect to that of the $\bar{B}_s^0 \rightarrow D^0K^{*0}$ candidates. The ratio of $B^\pm \rightarrow DK^\pm$ decays is determined using branching fractions, fragmentation fractions [39,40] and selection efficiencies in simulation, where differences from data are determined to be negligible. The ratio for misidentified $B^0 \rightarrow D\pi^+\pi^-$ decays is determined from the results of fits to $B^0 \rightarrow (D \rightarrow K\pi)K^{*0}$ decays. Finally, the combinatorial background is described by an exponential function, where the yield and slope are freely varying parameters in each category.

The projections of the global fits are displayed in Fig. 4. Table 1 details the yields of each component in a $30\text{ MeV}/c^2$ region either side of the B^0 mass [23]. The total signal yield and purity are 434 ± 32 and $(57 \pm 5)\%$, respectively. The dominant backgrounds in the signal region are from combinatorial candidates and $\bar{B}_s^0 \rightarrow D^{*0}K^{*0}$ decays. Other sources are negligible in comparison.

Simulation is used to verify that the component shapes do not vary across the Dalitz plot. Therefore, the same model is applied in the fit to extract the CP violation observables as for the global fit. The yield of each component, excluding combinatorial background, in a Dalitz plot bin is parameterised by the integrated yield multiplied by the expected fraction of candidates in that bin. For example, the distribution of signal candidates is described by Eqs. (12) and (13) where h_{B^0} and $h_{\bar{B}_s^0}$ are freely varying parameters.

In the fit, the CP violation observables are free parameters shared across all fit categories and the F_i [21], c_i , s_i [16,17] and κ [20] parameters are fixed.

The integrated yields of $\bar{B}_s^0 \rightarrow D^0K^{*0}$ decays are freely varying parameters in four categories given by the D decay mode and K_S^0 track type, whilst those of the remaining physics backgrounds are fixed to the results of the global fit. For each of the background components, excluding combinatorial background, the fractional yield in a Dalitz plot bin is fixed. The effect of CP violation in interference between the final state paths in $\bar{B}_s^0 \rightarrow D^0K^{*0}$ and $\bar{B}_s^0 \rightarrow D^{*0}K^{*0}$ decays is expected to be small because $r_{B_s^0} \sim 0.02$. Therefore, \bar{B}_s^0 particles are assumed to decay exclusively to D^0 mesons, thus

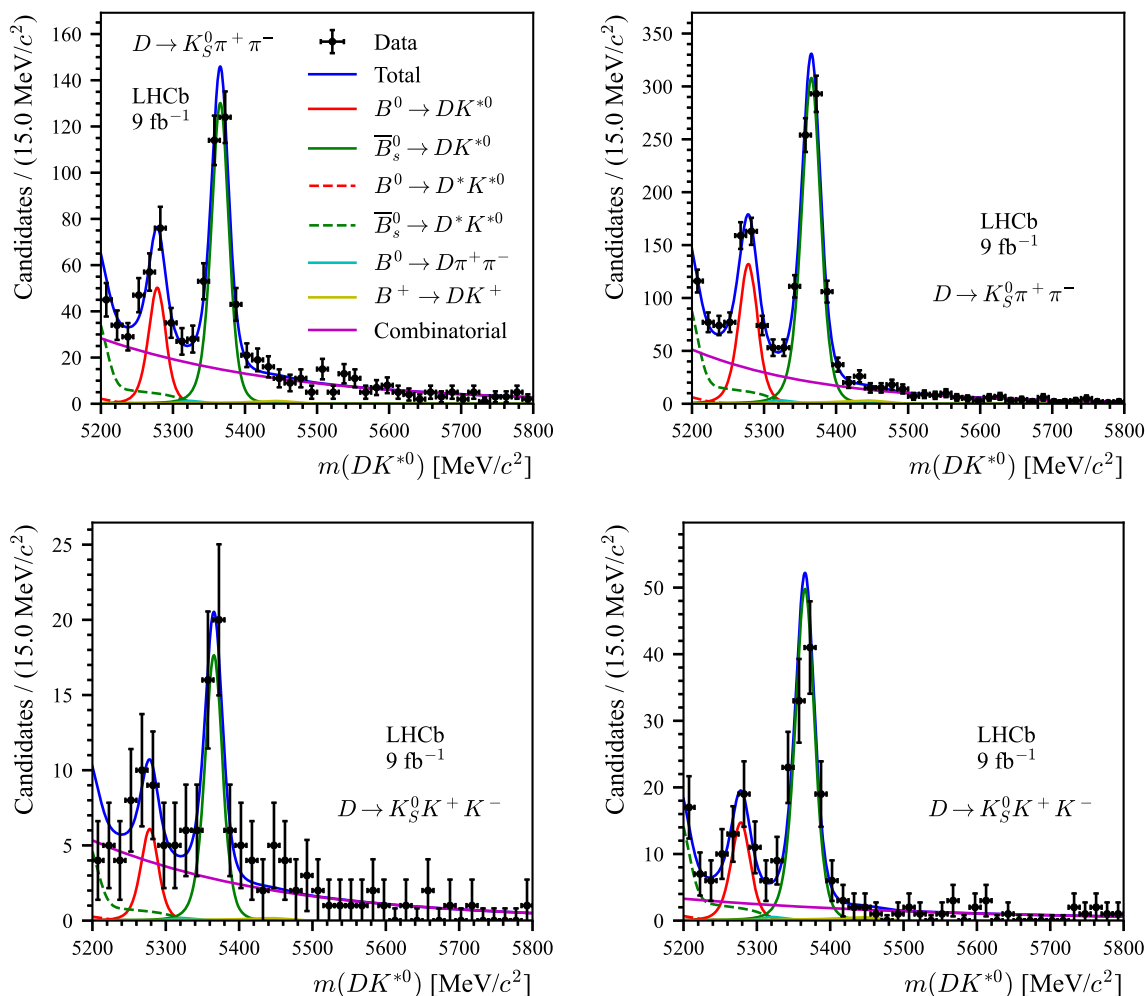


Fig. 4 Invariant-mass distributions of $B^0 \rightarrow DK^{*0}$ candidates with (upper) $D \rightarrow K_S^0 \pi^+ \pi^-$ and (lower) $D \rightarrow K_S^0 K^+ K^-$ decays, separated by the (left) long and (right) downstream K_S^0 track type. The data are overlaid with the global fit projection

Table 1 Yield of each component in a $30 \text{ MeV}/c^2$ region either side of the B^0 mass as determined by the global fit in four categories. Yields are either determined directly or through a combination of fit parameters.

The uncertainties are determined through propagation and further modulated by integration within the region. Some backgrounds have negligible yields in the aforementioned invariant-mass region

Component	$D \rightarrow K_S^0 \pi^+ \pi^-$ long	$D \rightarrow K_S^0 \pi^+ \pi^-$ downstream	$D \rightarrow K_S^0 K^+ K^-$ long	$D \rightarrow K_S^0 K^+ K^-$ downstream
$B^0 \rightarrow DK^{*0}$	102 ± 17	288 ± 25	12 ± 6	32 ± 8
$\bar{B}_s^0 \rightarrow D^0 K^{*0}$	2.4 ± 0.4	7.1 ± 0.6	0.32 ± 0.08	1.2 ± 0.2
Combinatorial	84 ± 8	133 ± 11	16 ± 3	11 ± 4
$\bar{B}_s^0 \rightarrow D^{*0} K^{*0}$	17.1 ± 1.4	44 ± 2	2.3 ± 0.5	7.1 ± 0.8
$B^0 \rightarrow D^* K^{*0}$	≤ 1	≤ 1	≤ 1	≤ 1
$B^0 \rightarrow D \pi^+ \pi^-$	≤ 1	1.8 ± 0.5	≤ 1	≤ 1
$B^\pm \rightarrow DK^\pm$	≤ 1	2.0 ± 0.4	≤ 1	≤ 1

the fraction of these candidates in a Dalitz plot bin is given by F_i . The level of CP violation in $B^0 \rightarrow D^*K^{*0}$ decays is likely at a similar level to the signal, but assigned as zero in the fit due to the very small yield of this decay in the fit range. Therefore, the fractional yield of this component in a Dalitz plot bin is F_{-i} . A systematic uncertainty is assigned for this assumption as discussed in Sect. 6. For the $B^0 \rightarrow D\pi^+\pi^-$ candidates, the D meson is assumed to be an equal mixture of D^0 and \bar{D}^0 mesons because either pion could be misidentified. Therefore, the fraction of these decays in a Dalitz plot bin is $0.5(F_i + F_{-i})$. The $B^\pm \rightarrow DK^\pm$ background is CP violating and its distribution over the Dalitz plot is therefore parameterised similarly to Eqs. (12) and (13) using values of the CP violation observables determined from Ref. [24], with $\kappa = 1$. Finally, the Dalitz plot distribution of combinatorial background is unknown, thus the corresponding yield in each bin is a free parameter.

After correcting for small biases (the largest of which is 12% of the statistical uncertainty) and uncertainty under-coverage (the largest inflation was 3%) using pseudoexperiments, the CP violation observables are measured to be $x_+ = 0.074 \pm 0.086$, $x_- = -0.215 \pm 0.086$, $y_+ = -0.336 \pm 0.105$ and $y_- = -0.012 \pm 0.128$, with the statistical correlation coefficients displayed in the Appendix. The left plot in Fig. 5 displays the 68.3% and 95.5% confidence regions for the CP violation observables determined by scanning the profile likelihood function. The opening angle between the lines joining the points (x_+, y_+) and (x_-, y_-) with the origin corresponds to 2γ . To understand the distribution of signal across the Dalitz plot the raw asymmetry, $N_i(\bar{B}^0) - N_{-i}(B^0)/N_i(\bar{B}^0) + N_{-i}(B^0)$, is calculated for each effective bin pair. An effective bin labelled i , is defined to compare the yield of \bar{B}^0 decays in a bin i with the yield of B^0 decays in a bin $-i$. Figure 5 displays the asymmetries calculated using the binned yields from the default fit, and for illustrative purposes, those determined in an alternative fit where the signal yield in each region of the Dalitz plot is a free parameter. The good agreement between the yield of signal in each bin determined from the CP violation observables and those determined from the alternative fit demonstrates that Eqs. (12) and (13) are an appropriate model for the data. It is possible to see regions of the Dalitz plot where the asymmetry does deviate from zero. However, CP violation in this measurement is not yet established with the current precision.

6 Systematic uncertainties

A summary of the systematic uncertainties is displayed in Table 2. These are primarily evaluated with two methods: the fit to the data is repeated many times using a model with fixed parameters smeared according to their uncertainties and

the root-mean-square (RMS) of the CP violation observable distributions are taken to be the uncertainties, or many pseudodata sets tuned to the data are fitted using a model with an alternative configuration and the biases in the CP violation observable distributions are taken to be the uncertainty.

Two systematic uncertainties are associated with the D decay strong-phase inputs. The effect of their finite precision is determined by generating a set of c_i and s_i values smeared according to their uncertainties and correlations. The corresponding systematic uncertainties are 0.005, 0.004, 0.017 and 0.024 for x_+ , x_- , y_+ and y_- , respectively. These are larger for y_\pm because the s_i values are known less precisely than those of c_i , but they remain significantly smaller than the statistical uncertainties.

An uncertainty arises because the effect of $\eta(m_-^2, m_+^2)$ is not accounted for in the D decay strong-phase parameters. Alternative c_i and s_i are calculated using an amplitude model [41] with a flat efficiency profile (c_i^{flat} , s_i^{flat}) and an efficiency profile determined using simulated signal decays (c_i^{eff} , s_i^{eff}). The subsequent systematic uncertainty is evaluated by fitting the data many times using a model with alternative c_i and s_i coefficients that are generated from a Gaussian with a width equal to the efficiency correction: $\delta c_i = c_i^{\text{flat}} - c_i^{\text{eff}}$ and $\delta s_i = s_i^{\text{flat}} - s_i^{\text{eff}}$.

Selection differences between $B^0 \rightarrow DK^{*0}$ and $B^\pm \rightarrow D\pi^\pm$ candidates can alter the relative efficiencies in each Dalitz plot bin, introducing a bias on the F_i parameters appropriate for these decay channels. The ratio of the squared $(\pi^+\pi^-)_D$ invariant-mass distribution in simulated $B^0 \rightarrow DK^{*0}$ and $B^\pm \rightarrow D\pi^\pm$ decays are used to produce an alternative efficiency profile. This is subsequently applied to an amplitude model [41] to compute different F_i values. The relative efficiency differences between signal and $\bar{B}_s^0 \rightarrow D^0K^{*0}$ decays are negligible. It is the dominant systematic uncertainty for the x_\pm observables, but is significantly lower than the equivalent uncertainty determined in Ref. [11] where the efficiency profile from $B^0 \rightarrow D^{*-}\mu^+\nu_\mu$ decays was used.

Various systematic uncertainties related to the fit model are computed. The dominant contributions are the choice of signal shape and the effect of fixing the combinatorial background slope, signal mean and resolution to the global fit results, and are both evaluated using alternative models. In the former a different signal distribution is used, and in the latter the slopes in each of the four global fit categories are freely varying parameters that are shared between Dalitz plot bins. The remaining fit model systematics are those associated with the fixed background ratios, which are evaluated using sets of parameters smeared according to their uncertainties.

In the fit model, CP violation in partially reconstructed $B^0 \rightarrow D^*K^{*0}$ decays is neglected because there are few candidates in the fit range. The effect of this assumption is measured using an alternative model where these candidates have

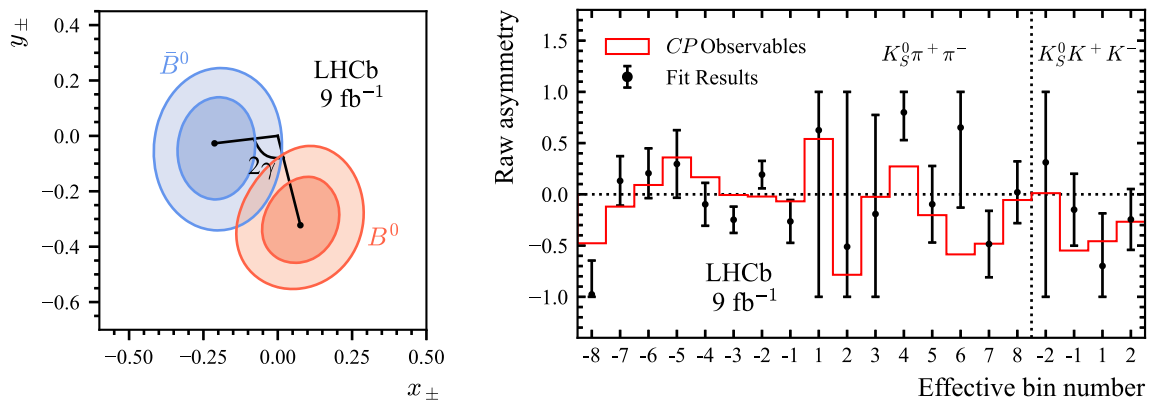


Fig. 5 Left: two-dimensional 68.3% and 95.5% statistical confidence regions for the measured (x_{\pm}, y_{\pm}) values, determined by scanning the profile likelihood function. The blue (orange) contours correspond to the observables related to B^0 (\bar{B}^0) decays. Right: raw asymmetry in each effective bin pair. It is determined using the fitted CP violation

observables (red histogram) and the results of an alternative fit where the signal yield in each Dalitz plot bin is a free parameter (black points, with statistical uncertainties that are capped to the physical limits where appropriate)

Table 2 Systematic uncertainties for the CP violation observables. Statistical uncertainties are given for reference

Source	$\sigma(x_+)$	$\sigma(x_-)$	$\sigma(y_+)$	$\sigma(y_-)$
Efficiency correction of (c_i, s_i)	0.001	0.001	0.002	0.001
F_i inputs	0.006	0.007	0.001	0.000
Mass Fit	0.002	0.006	0.005	0.004
$B^0 \rightarrow D^* K^{*0}$ CP violation	0.001	0.001	0.001	0.001
Value of κ	0.000	0.001	0.003	0.002
Charmless background	0.009	0.008	0.000	0.005
Bin migration	0.001	0.001	0.000	0.002
Fitter bias	0.003	0.003	0.006	0.004
Total of above systematics	0.011	0.013	0.009	0.011
Strong-phase measurements	0.005	0.004	0.017	0.024
Statistical uncertainty	0.086	0.086	0.105	0.128

the same distribution in phase space as the signal decays. The amplitude ratio and strong-phase difference for these decays are unknown, but a similar interference as in $B^0 \rightarrow DK^{*0}$ decays is expected since they have a similar amplitude ratio. Hence, the CP violation observables determined by the nominal fit are used and the resulting uncertainty is small.

The systematic uncertainty associated with the limited knowledge of the coherence factor, κ , is determined to be small using an alternative model where its value is displaced by one standard deviation, $\kappa_{\text{model}} = \kappa - \sigma(\kappa)$ [20]. Larger values of κ are not included since its uncertainty is heavily asymmetric, and the lower uncertainty is found to dominate the spread of CP violation observables.

In the selection, a requirement is placed on the displacement of the D meson vertex from the B meson vertex to reduce background from B decays to the final state particles without the intermediate D meson, which are referred to as

charmless candidates. Studies of the D meson invariant-mass sideband determine that the total charmless yield in the sample is 17 ± 9 . A systematic uncertainty is assigned using an alternative model where charmless candidates are introduced in the signal region. The yields of these candidates are distributed uniformly over the Dalitz plot and given the small expected yields it is unnecessary to account for potential CP violation in the charmless decays.

Measurements of the Dalitz plot coordinates are affected by the detector momentum resolution and can cause candidates to be assigned to the wrong bin. To first order, the F_i values account for this, but the net migration between Dalitz plot bins can differ in $B^{\pm} \rightarrow D\pi^{\pm}$ and $B^0 \rightarrow DK^{*0}$ decays since they exhibit different levels of CP violation. The expected difference in the F_i values in $B^{\pm} \rightarrow D\pi^{\pm}$ and $B^0 \rightarrow DK^{*0}$ due to these second order effects is determined using the momentum resolution in simulation, the CP viola-

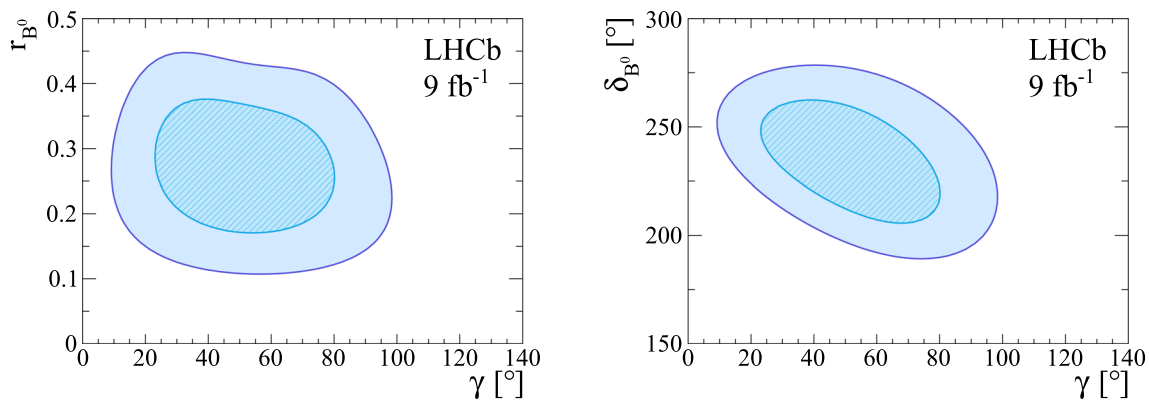


Fig. 6 Profile likelihood contours for (left) γ versus r_{B^0} and (right) γ versus δ_{B^0} corresponding to 68.3% and 95.5% confidence regions

tion observables of $B^\pm \rightarrow D\pi^\pm$ [24] and those of this analysis and the D decay model from Ref. [41]. The expected differences are used to generate pseudoexperiments which are then fit with the nominal procedure to assign the systematic uncertainty due to momentum resolution.

The corrections applied to the CP violation observables in Sect. 5 depend on the physics inputs used in the pseudo-data studies. Therefore, a systematic uncertainty is assigned. The values of and correlations between γ , r_{B^0} and δ_{B^0} from Ref. [24] are used to generate sets of alternative input CP violation observables. The bias study is repeated many times to create a distribution of corrections, the RMS of which corresponds to the systematic uncertainty.

The total systematic uncertainties from all sources excluding those associated with the limited knowledge of the c_i and s_i coefficients is determined by summing all the contributions in quadrature. They are 0.011, 0.013, 0.009 and 0.011 for x_+ , x_- , y_+ and y_- , respectively, and their correlations are given in the Appendix.

7 Interpretation

The CP violation observables are determined to be

$$\begin{aligned} x_+ &= 0.074 \pm 0.086 \pm 0.005 \pm 0.011, \\ x_- &= -0.215 \pm 0.086 \pm 0.004 \pm 0.013, \\ y_+ &= -0.336 \pm 0.105 \pm 0.017 \pm 0.009, \\ y_- &= -0.012 \pm 0.128 \pm 0.024 \pm 0.011, \end{aligned}$$

where the first uncertainty is statistical, the second is the systematic contribution from the D decay strong-phase inputs and the third is from the experimental systematic uncertainties. The measured CP violation observables are used in a maximum likelihood fit to determine the physics parameters γ , r_{B^0} and δ_{B^0} . The CP violation observables are invariant under the transformation $\gamma \rightarrow \gamma + 180^\circ$ and $\delta_{B^0} \rightarrow \delta_{B^0} + 180^\circ$ which leads to two unambiguous solutions for the physics observables. In the region where $0 < \gamma < 180^\circ$

is satisfied, the best fit values are

$$\begin{aligned} \gamma &= (49_{-19}^{+22})^\circ, \\ r_{B^0} &= 0.271_{-0.066}^{+0.065}, \\ \delta_{B^0} &= (236_{-21}^{+19})^\circ, \end{aligned}$$

where the uncertainties are calculated using a frequentist method described in Ref. [24]. The corresponding 68.3% and 95.5% confidence regions in the γ vs. r_{B^0} and γ vs. δ_{B^0} planes are displayed in Fig. 6.

In the most recent combination of LHCb results [24], the mean value of γ determined using the $B^0 \rightarrow DK^{*0}$ channel was $\gamma = (82.0_{-8.8}^{+8.1})^\circ$, which is higher than the average value using B^\pm decays, $\gamma = (61.7_{-4.8}^{+4.4})^\circ$. The value of γ presented here is in good agreement with the current LHCb average, $\gamma = (65.4_{-4.2}^{+3.8})^\circ$ [24], and will reduce the difference between measurements performed using different b -mesons. Furthermore, it is compatible with the value measured in Ref. [11], $\gamma = (71 \pm 20)^\circ$, although there is not a substantial precision improvement despite using a larger data set. This is explained by noting that the uncertainty on γ is inversely proportional to the value of r_{B^0} , which had a higher central value in Ref. [11] than the current measurement. The value of r_{B^0} presented in this paper is consistent with previous determinations from LHCb [10], BaBar [9] and Belle [7, 8]. The precision of the CP violation observables have significantly improved and therefore the results presented here will have a larger weight in future γ combinations.

8 Summary

Proton-proton collision data corresponding to an integrated luminosity of 9 fb^{-1} collected by the LHCb experiment at centre-of-mass energies of $\sqrt{s} = 7, 8$ and 13 TeV are used to perform a binned, model-independent CP violation study of $B^0 \rightarrow DK^{*0}$ decays to measure the CKM angle γ . Strong-phase information of $D \rightarrow K_S^0 h^+ h^-$ decays (where

$h = \pi, K$) from the CLEO [19] and BESIII [16–18] experiments is used as inputs. The measured value is $\gamma = (49_{-19}^{+22})^\circ$, where the uncertainty is statistically dominated and systematic contributions are an order of magnitude smaller. The CP violation observables measured here are consistent with and supersede those presented in Ref. [11].

Acknowledgements We express our gratitude to our colleagues in the CERN accelerator departments for the excellent performance of the LHC. We thank the technical and administrative staff at the LHCb institutes. We acknowledge support from CERN and from the national agencies: CAPES, CNPq, FAPERJ and FINEP (Brazil); MOST and NSFC (China); CNRS/IN2P3 (France); BMBF, DFG and MPG (Germany); INFN (Italy); NWO (Netherlands); MNiSW and NCN (Poland); MEN/IFA (Romania); MICINN (Spain); SNSF and SER (Switzerland); NASU (Ukraine); STFC (United Kingdom); DOE NP and NSF (USA). We acknowledge the computing resources that are provided by CERN, IN2P3 (France), KIT and DESY (Germany), INFN (Italy), SURF (Netherlands), PIC (Spain), GridPP (United Kingdom), CSCS (Switzerland), IFIN-HH (Romania), CBPF (Brazil), Polish WLCG (Poland) and NERSC (USA). We are indebted to the communities behind the multiple open-source software packages on which we depend. Individual groups or members have received support from ARC and ARDC (Australia); Minciencias (Colombia); AvH Foundation (Germany); EPLANET, Marie Skłodowska-Curie Actions, ERC and NextGenerationEU (European Union); A*MIDEX, ANR, IPhU and Labex P2IO, and Région Auvergne-Rhône-Alpes (France); Key Research Program of Frontier Sciences of CAS, CAS PIFI, CAS CCEPP, Fundamental Research Funds for the Central Universities, and Sci. and Tech. Program of Guangzhou (China); GVA, XuntaGal, GENCAT, Inditex, InTalent and Prog. Atracción Talento, CM (Spain); SRC (Sweden); the Leverhulme Trust, the Royal Society and UKRI (United Kingdom).

Data availability This manuscript has no associated data or the data will not be deposited. [Authors' comment: All LHCb scientific output is published in journals, with preliminary results made available in Conference Reports. All are Open Access, without restriction on use beyond the standard conditions agreed by CERN. Data associated to the plots in this publication as well as in supplementary materials are made available on the CERN document server at <https://cds.cern.ch/record/2870359>. This information is taken from the LHCb External Data Access Policy which can be downloaded at <http://opendata.cern.ch/record/410>.]

Open Access This article is licensed under a Creative Commons Attribution 4.0 International License, which permits use, sharing, adaptation, distribution and reproduction in any medium or format, as long as you give appropriate credit to the original author(s) and the source, provide a link to the Creative Commons licence, and indicate if changes were made. The images or other third party material in this article are included in the article's Creative Commons licence, unless indicated otherwise in a credit line to the material. If material is not included in the article's Creative Commons licence and your intended use is not permitted by statutory regulation or exceeds the permitted use, you will need to obtain permission directly from the copyright holder. To view a copy of this licence, visit <http://creativecommons.org/licenses/by/4.0/>.
Funded by SCOAP³.

Appendix: Correlation matrices

Tables 3 and 4 display the correlation coefficients between the statistical and systematic uncertainties (excluding the strong-phase inputs) on the CP violation observables, respectively.

A systematic uncertainty is assigned to account for the finite precision on the D decay strong-phase inputs, c_i and s_i [16, 17]. It is given by the RMS of the distributions of CP violation observables obtained from fitting the data many times using a model with c_i and s_i values that are smeared according to their uncertainties and correlations. This procedure is common between model-independent γ measurements. Therefore, the alternative c_i and s_i used for this study are taken from an analysis of $B^\pm \rightarrow Dh^\pm$ decays at LHCb [21], which allows correlation coefficients between CP violation observables of both analysis to be computed. Thus, in combinations the correlation of this systematic uncertainty can be accounted for. These are displayed in Table 5.

Table 3 Statistical correlation matrix for the CP violation observables

	x_+	x_-	y_+	y_-
x_+	1.00	0.00	0.18	0.00
x_-		1.00	0.00	0.08
y_+			1.00	0.00
y_-				1.00

Table 4 Correlations between the CP violation observables for systematic uncertainties excluding the strong-phase inputs

	x_+	x_-	y_+	y_-
x_+	1.00	-0.02	0.05	0.00
x_-		1.00	0.05	0.04
y_+			1.00	-0.07
y_-				1.00

Table 5 Correlations in the CP violation observables for the strong-phase related systematic uncertainties in $B^0 \rightarrow DK^{*0}$ and $B^\pm \rightarrow Dh^\pm$ [21]

	$x_+^{DK^{*0}}$	$x_-^{DK^{*0}}$	$y_+^{DK^{*0}}$	$y_-^{DK^{*0}}$	x_-^{DK}	x_+^{DK}	y_-^{DK}	y_+^{DK}	$x_\xi^{D\pi}$	$y_\xi^{D\pi}$
$x_+^{DK^{*0}}$	1.00	-0.14	0.34	-0.09	-0.29	-0.06	-0.11	-0.06	-0.16	0.30
$x_-^{DK^{*0}}$		1.00	-0.04	0.17	-0.31	0.48	0.22	-0.49	0.04	0.12
$y_+^{DK^{*0}}$			1.00	-0.04	0.35	0.03	0.12	0.27	0.29	0.32
$y_-^{DK^{*0}}$				1.00	0.13	-0.15	0.22	-0.01	0.21	0.36
x_-^{DK}					1.00	-0.49	-0.05	0.32	0.19	0.14
x_+^{DK}						1.00	0.06	0.06	0.00	-0.14
y_-^{DK}							1.00	-0.24	-0.12	-0.12
y_+^{DK}								1.00	0.12	-0.20
$x_\xi^{D\pi}$									1.00	0.64
$y_\xi^{D\pi}$										1.00

References

- N. Cabibbo, Unitary symmetry and leptonic decays. Phys. Rev. Lett. **10**, 531 (1963). <https://doi.org/10.1103/PhysRevLett.10.531>
- M. Kobayashi, T. Maskawa, CP-violation in the renormalizable theory of weak interaction. Prog. Theor. Phys. **49**, 652 (1973). <https://doi.org/10.1143/PTP.49.652>
- J. Brod, J. Zupan, The ultimate theoretical error on γ from $B \rightarrow DK$ decays. JHEP **01**, 051 (2014). [https://doi.org/10.1007/JHEP01\(2014\)051](https://doi.org/10.1007/JHEP01(2014)051). arXiv:1308.5663
- Y. Amhis et al., Averages of b -hadron, c -hadron, and τ -lepton properties as of 2021. Phys. Rev. D **107**, 052008. <https://doi.org/10.1103/PhysRevD.107.052008>. arXiv:2206.07501, updated results and plots available at <https://hflav.web.cern.ch> (2023)
- J. Charles et al., CKMfitter Group, Current status of the standard model CKM fit and constraints on $\Delta F = 2$ new physics. Phys. Rev. D **91**, 073007. <https://doi.org/10.1103/PhysRevD.91.073007>. arXiv:1501.05013, updated results and plots available at <http://ckmfitter.in2p3.fr/> (2015)
- M. Bona et al., UFit Collaboration, New UFit Analysis of the unitarity triangle in the Cabibbo–Kobayashi–Maskawa scheme. Rend. Lincei Sci. Fis. Nat. **34**, 37 (2023). <https://doi.org/10.1007/s12210-023-01137-5>. arXiv:2212.03894
- K. Negishi et al., Belle Collaboration, Search for the decay $B^0 \rightarrow DK^{*0}$ followed by $D \rightarrow K^- \pi^+$. Phys. Rev. D **86**, 011101 (2012). <https://doi.org/10.1103/PhysRevD.86.011101>. arXiv:1205.0422
- K. Negishi et al., Belle Collaboration, First model-independent Dalitz analysis of $B^0 \rightarrow DK^{*0}$, $D \rightarrow K_S^0 \pi^+ \pi^-$ decay. PTEP **2016**, 043C01 (2016). <https://doi.org/10.1093/ptep/ptw030>. arXiv:1509.01098
- B. Aubert et al., BABAR Collaboration, Search for $b \rightarrow u$ transitions in $B^0 \rightarrow D^0 K^{*0}$ decays. Phys. Rev. D **80**, 031102 (2009). <https://doi.org/10.1103/PhysRevD.80.031102>
- R. Aaij et al., LHCb Collaboration, Measurement of CP observables in the process $B^0 \rightarrow DK^{*0}$ with two- and four-body D decays. JHEP **08**, 041 (2019). [https://doi.org/10.1007/JHEP08\(2019\)041](https://doi.org/10.1007/JHEP08(2019)041). arXiv:1906.08297
- R. Aaij et al., LHCb Collaboration, Model-independent measurement of the CKM angle γ using $B^0 \rightarrow DK^{*0}$ decays with $D \rightarrow K_S^0 \pi^+ \pi^-$ and $K_S^0 K^+ K^-$. JHEP **06**, 131 (2016). [https://doi.org/10.1007/JHEP06\(2016\)131](https://doi.org/10.1007/JHEP06(2016)131). arXiv:1604.01525
- A. Bondar, *Proceedings of BINP Special Analysis Meeting on Dalitz Analysis*, unpublished (2022)
- A. Bondar, A. Poluektov, Feasibility study of model-independent approach to ϕ_3 measurement using Dalitz plot analysis. Eur. Phys. J. C **47**, 347 (2006). <https://doi.org/10.1140/epjc/s2006-02590-x>. arXiv:hep-ph/0510246
- A. Bondar, A. Poluektov, The use of quantum-correlated D^0 decays for ϕ_3 measurement. Eur. Phys. J. C **55**, 51 (2008). <https://doi.org/10.1140/epjc/s10052-008-0600-z>. arXiv:0801.0840
- A. Giri, Y. Grossman, A. Soffer, J. Zupan, Determining γ using $B^\pm \rightarrow DK^\pm$ with multibody D decays. Phys. Rev. D **68**, 054018 (2003). <https://doi.org/10.1103/PhysRevD.68.054018>. arXiv:hep-ph/0303187
- M. Ablikim et al., BESIII Collaboration, Model-independent determination of the relative strong-phase difference between D^0 and $\bar{D}^0 \rightarrow K_{S,L}^0 \pi^+ \pi^-$ and its impact on the measurement of the CKM angle γ/ϕ_3 . Phys. Rev. D **101**, 112002 (2020). <https://doi.org/10.1103/PhysRevD.101.112002>. arXiv:2003.00091
- M. Ablikim et al., BESIII Collaboration, Improved model-independent determination of the strong-phase difference between D^0 and $\bar{D}^0 \rightarrow K_{S,L}^0 K^+ K^-$ decays. Phys. Rev. D **102**, 052008 (2020). <https://doi.org/10.1103/PhysRevD.102.052008>. arXiv:2007.07959
- M. Ablikim et al., BESIII Collaboration, Determination of strong-phase parameters in $D \rightarrow K_{S,L}^0 \pi^+ \pi^-$. Phys. Rev. Lett. **124**, 241802 (2020). <https://doi.org/10.1103/PhysRevLett.124.241802>. arXiv:2002.12791
- J. Libby et al., CLEO Collaboration, Model-independent determination of the strong-phase difference between D^0 and $\bar{D}^0 \rightarrow K_{S,L}^0 h^+ h^-$ ($h = \pi, K$) and its impact on the measurement of the CKM angle γ/ϕ_3 . Phys. Rev. D **82**, 112006 (2010). <https://doi.org/10.1103/PhysRevD.82.112006>. arXiv:1010.2817
- R. Aaij et al., LHCb Collaboration, Constraints on the unitarity triangle angle γ from Dalitz plot analysis of $B^0 \rightarrow DK^+ \pi^-$ decays. Phys. Rev. D **93**, 112018 (2016). <https://doi.org/10.1103/PhysRevD.93.112018>. arXiv:1602.03455 [Erratum *ibid.* D **94**, 079902, 2016, <https://doi.org/10.1103/PhysRevD.94.079902>]
- R. Aaij et al., LHCb Collaboration, Measurement of the CKM angle γ in $B^\pm \rightarrow DK^\pm$ and $B^\pm \rightarrow D\pi^\pm$ decays with $D \rightarrow K_S h^+ h^-$. JHEP **02**, 0169 (2021). [https://doi.org/10.1007/JHEP02\(2021\)169](https://doi.org/10.1007/JHEP02(2021)169). arXiv:2010.08483
- B. Aubert et al., BaBar Collaboration, Measurement of γ in $B^\mp \rightarrow D^{(*)} K^\mp$ decays with a Dalitz analysis of $D \rightarrow K_S^0 \pi^- \pi^+$. Phys. Rev. Lett. **95**, 121802 (2005). <https://doi.org/10.1103/PhysRevLett.95.121802>. arXiv:hep-ex/0504039
- R.L. Workman et al., Particle Data Group, Review of particle physics. Prog. Theor. Exp. Phys. **2022**, 083C01 (2022). <https://doi.org/10.1093/ptep/ptac097>

24. LHCb Collaboration, R. Aaij et al., Simultaneous determination of CKM angle γ and charm mixing parameters. *JHEP* **12**, 141 (2021). [https://doi.org/10.1007/JHEP12\(2021\)141](https://doi.org/10.1007/JHEP12(2021)141). arXiv:2110.02350
25. LHCb Collaboration, A.A. Alves et al., The LHCb detector at the LHC. *JINST* **3**, S08005 (2008). <https://doi.org/10.1088/1748-0221/3/08/S08005>
26. LHCb Collaboration, R. Aaij et al., LHCb detector performance. *Int. J. Mod. Phys. A* **30**, 1530022 (2015). <https://doi.org/10.1142/S0217751X15300227>. arXiv:1412.6352
27. V.V. Gligorov, M. Williams, Efficient, reliable and fast high-level triggering using a bonsai boosted decision tree. *JINST* **8**, P02013 (2013). <https://doi.org/10.1088/1748-0221/8/02/P02013>. arXiv:1210.6861
28. T. Sjöstrand, S. Mrenna, P. Skands, A brief introduction to PYTHIA 8.1. *Comput. Phys. Commun.* **178**, 852 (2008). <https://doi.org/10.1016/j.cpc.2008.01.036>. arXiv:0710.3820
29. T. Sjöstrand, S. Mrenna, P. Skands, PYTHIA 6.4 physics and manual. *JHEP* **05**, 026 (2006). <https://doi.org/10.1088/1126-6708/2006/05/026>. arXiv:hep-ph/0603175
30. I. Belyaev et al., Handling of the generation of primary events in Gauss, the LHCb simulation framework. *J. Phys. Conf. Ser.* **331**, 032047 (2011). <https://doi.org/10.1088/1742-6596/331/3/032047>
31. D.J. Lange, The EvtGen particle decay simulation package. *Nucl. Instrum. Meth.* **A462**, 152 (2001). [https://doi.org/10.1016/S0168-9002\(01\)00089-4](https://doi.org/10.1016/S0168-9002(01)00089-4)
32. N. Davidson, T. Przedzinski, Z. Was, PHOTOS interface in C++: technical and physics documentation. *Comput. Phys. Commun.* **199**, 86 (2016). <https://doi.org/10.1016/j.cpc.2015.09.013>. arXiv:1011.0937
33. Geant4 Collaboration, J. Allison et al., Geant4 developments and applications. *IEEE Trans. Nucl. Sci.* **53**, 270 (2006). <https://doi.org/10.1109/TNS.2006.869826>
34. Geant4 Collaboration, S. Agostinelli et al., Geant4: a simulation toolkit. *Nucl. Instrum. Meth. A* **506**, 250 (2003). [https://doi.org/10.1016/S0168-9002\(03\)01368-8](https://doi.org/10.1016/S0168-9002(03)01368-8)
35. M. Clemencic et al., The LHCb simulation application, Gauss: design, evolution and experience. *J. Phys. Conf. Ser.* **331**, 032023 (2011). <https://doi.org/10.1088/1742-6596/331/3/032023>
36. L. Breiman, J.H. Friedman, R.A. Olshen, C.J. Stone, *Classification and Regression Trees* (Wadsworth International Group, Belmont, 1984)
37. Y. Freund, R.E. Schapire, A decision-theoretic generalization of on-line learning and an application to boosting. *J. Comput. Syst. Sci.* **55**, 119 (1997). <https://doi.org/10.1006/jcss.1997.1504>
38. LHCb Collaboration, R. Aaij et al., Observation of the $B^0 \rightarrow \bar{D}^{*0} K^+ \pi^-$ and $B_s^0 \rightarrow \bar{D}^{*0} K^- \pi^+$ decays. *Phys. Rev. D* **105**, 072005 (2022). <https://doi.org/10.1103/PhysRevD.105.072005>. arXiv:2112.11428
39. LHCb Collaboration, R. Aaij et al., Measurement of the fragmentation fraction ratio f_s/f_d and its dependence on B meson kinematics. *JHEP* **04**, 001 (2013). [https://doi.org/10.1007/JHEP04\(2013\)001](https://doi.org/10.1007/JHEP04(2013)001). arXiv:1301.5286
40. LHCb Collaboration, R. Aaij et al., Precise measurement of the f_s/f_d ratio of fragmentation fractions and of B_s^0 decay branching fractions. *Phys. Rev. D* **104**, 032005 (2021). <https://doi.org/10.1103/PhysRevD.104.032005>. arXiv:2103.06810
41. BaBar, Belle Collaborations, I. Adachi et al., Measurement of $\cos 2\beta$ in $B^0 \rightarrow D^{(*)} h^0$ with $D \rightarrow K_S^0 \pi^+ \pi^-$ decays by a combined time-dependent Dalitz plot analysis of BaBar and Belle data. *Phys. Rev. D* **98**, 112012 (2018). <https://doi.org/10.1103/PhysRevD.98.112012>. arXiv:1804.06153

LHCb collaboration*

R. Aaij³², A. S. W. Abdelmotteleb⁵¹, C. Abellan Beteta⁴⁵, F. Abudinén⁵¹, T. Ackernley⁵⁵, B. Adeva⁴¹, M. Adinolfi⁴⁹, P. Adlarson⁷⁷, H. Afsharnia⁹, C. Agapopoulou⁴³, C. A. Aidala⁷⁸, Z. Ajaltouni⁹, S. Akar⁶⁰, K. Akiba³², P. Albicocco²³, J. Albrecht¹⁵, F. Alessio⁴³, M. Alexander⁵⁴, A. Alfonso Alberio⁴⁰, Z. Aliouche⁵⁷, P. Alvarez Cartelle⁵⁰, R. Amalric¹³, S. Amato², J. L. Amey⁴⁹, Y. Amhis^{11,43}, L. An⁵, L. Anderlini²², M. Andersson⁴⁵, A. Andreianov³⁸, P. A. Andreola⁴⁵, M. Andreotti²¹, D. Andreou⁶³, D. Ao⁶, F. Archilli^{31,t}, A. Artamonov³⁸, M. Artuso⁶³, E. Aslanides¹⁰, M. Atzeni⁴⁵, B. Audurier¹², I. B. Bachiller Perea⁸, S. Bachmann¹⁷, M. Bachmayer⁴⁴, J. J. Back⁵¹, A. Bailly-reyre¹³, P. Baladron Rodriguez⁴¹, V. Balagura¹², W. Baldini^{21,43}, J. Baptista de Souza Leite¹, M. Barbeti^{22,j}, I. R. Barbosa⁶⁵, R. J. Barlow⁵⁷, S. Barsuk¹¹, W. Barter⁵³, M. Bartolini⁵⁰, F. Baryshnikov³⁸, J. M. Basels¹⁴, G. Bassi^{29,q}, B. Batsukh⁴, A. Battig¹⁵, A. Bay⁴⁴, A. Beck⁵¹, M. Becker¹⁵, F. Bedeschi²⁹, I. B. Bediaga¹, A. Beiter⁶³, S. Belin⁴¹, V. Bellee⁴⁵, K. Belous³⁸, I. Belov²⁴, I. Belyaev³⁸, G. Benane¹⁰, G. Bencivenni²³, E. Ben-Haim¹³, A. Berezhnoy³⁸, R. Bernet⁴⁵, S. Bernet Andres³⁹, D. Berninghoff¹⁷, H. C. Bernstein⁶³, C. Bertella⁵⁷, A. Bertolin²⁸, C. Betancourt⁴⁵, F. Betti⁴³, Ia. Bezshyiko⁴⁵, J. Bhom³⁵, L. Bian⁶⁹, M. S. Bieker¹⁵, N. V. Biesuz²¹, P. Billoir¹³, A. Biolchini³², M. Birch⁵⁶, F. C. R. Bishop⁵⁰, A. Bitadze⁵⁷, A. Bizzeti, M. P. Blago⁵⁰, T. Blake⁵¹, F. Blanc⁴⁴, J. E. Blank¹⁵, S. Blusk⁶³, D. Bobulska⁵⁴, V. B. Bocharnikov³⁸, J. A. Boelhauve¹⁵, O. Boente Garcia¹², T. Boettcher⁶⁰, A. Bohare⁵³, A. Boldyrev³⁸, C. S. Bolognani⁷⁵, R. Bolzonella^{21,i}, N. Bondar³⁸, F. Borgato^{28,43}, S. Borghi⁵⁷, M. Borsato¹⁷, J. T. Borsuk³⁵, S. A. Bouchiba⁴⁴, T. J. V. Bowcock⁵⁵, A. Boyer⁴³, C. Bozzi²¹, M. J. Bradley⁵⁶, S. Braun⁶¹, A. Brea Rodriguez⁴¹, N. Breer¹⁵, J. Brodzicka³⁵, A. Brossa Gonzalo⁴¹, J. Brown⁵⁵, D. Brundu²⁷, A. Buonaura⁴⁵, L. Buonincontri²⁸, A. T. Burke⁵⁷, C. Burr⁴³, A. Bursche⁶⁷, A. Butkevich³⁸, J. S. Butter³², J. Buytaert⁴³, W. Byczynski⁴³, S. Cadeddu²⁷, H. Cai⁶⁹, R. Calabrese^{21,i}, L. Calefice¹⁵, S. Cali²³, M. Calvi^{26,m}, M. Calvo Gomez³⁹, P. Campana²³, D. H. Campora Perez⁷⁵, A. F. Campoverde Quezada⁶, S. Capelli^{26,m}, L. Capriotti²¹, A. Carbone^{20,g}, R. Cardinale^{24,k}, A. Cardini²⁷

P. Carniti^{26,m}, L. Carus¹⁷, A. Casais Vidal⁴¹, R. Caspary¹⁷, G. Casse⁵⁵, M. Cattaneo⁴³, G. Cavallero²¹, V. Cavallini^{21,i}, S. Celani⁴⁴, J. Cerasoli¹⁰, D. Cervenkov⁵⁸, A. J. Chadwick⁵⁵, I. C. Chahrour⁷⁸, M. G. Chapman⁴⁹, M. Charles¹³, Ph. Charpentier⁴³, C. A. Chavez Barajas⁵⁵, M. Chefdeville⁸, C. Chen¹⁰, S. Chen⁴, A. Chernov³⁵, S. Chernyshenko⁴⁷, V. Chobanova^{41,w}, S. Cholak⁴⁴, M. Chrzaszcz³⁵, A. Chubykin³⁸, V. Chulikov³⁸, P. Ciambrone²³, M. F. Cicala⁵¹, X. Cid Vidal⁴¹, G. Ciezarek⁴³, P. Cifra⁴³, G. Ciullo^{21,i}, P. E. L. Clarke⁵³, M. Clemencic⁴³, H. V. Cliff⁵⁰, J. Closier⁴³, J. L. Cobbedick⁵⁷, V. Coco⁴³, J. Cogan¹⁰, E. Cogneras⁹, L. Cojocariu³⁷, P. Collins⁴³, T. Colombo⁴³, A. Comerma-Montells⁴⁰, L. Congedo¹⁹, A. Contu²⁷, N. Cooke⁵⁴, I. Corredoira⁴¹, G. Corti⁴³, J. J. Cottee Meldrum⁴⁹, B. Couturier⁴³, D. C. Craik⁴⁵, M. Cruz Torres^{1,e}, R. Currie⁵³, C. L. Da Silva⁶², S. Dadabaev³⁸, L. Dai⁶⁶, X. Dai⁵, E. Dall'Occo¹⁵, J. Dalseno⁴¹, C. D'Ambrosio⁴³, J. Daniel⁹, A. Danilina³⁸, P. d'Argent¹⁹, J. E. Davies⁵⁷, A. Davis⁵⁷, O. De Aguiar Francisco⁵⁷, J. de Boer³², K. De Bruyn⁷⁴, S. De Capua⁵⁷, M. De Cian¹⁷, U. De Freitas Carneiro Da Graca¹, E. De Lucia²³, J. M. De Miranda¹, L. De Paula², M. De Serio^{19,f}, D. De Simone⁴⁵, P. De Simone²³, F. De Vellis¹⁵, J. A. de Vries⁷⁵, C. T. Dean⁶², F. Debernardis^{19,f}, D. Decamp⁸, V. Dedu¹⁰, L. Del Buono¹³, B. Delaney⁵⁹, H.-P. Dembinski¹⁵, V. Denysenko⁴⁵, O. Deschamps⁹, F. Dettori^{27,h}, B. Dey⁷², P. Di Nezza²³, I. Diachkov³⁸, S. Didenko³⁸, S. Ding⁶³, V. Dobishuk⁴⁷, A. Dolmatov³⁸, C. Dong³, A. M. Donohoe¹⁸, F. Dordei²⁷, A. C. dos Reis¹, L. Douglas⁵⁴, A. G. Downes⁸, W. Duan⁶⁷, P. Duda⁷⁶, M. W. Dudek³⁵, L. Dufour⁴³, V. Duk⁷³, P. Durante⁴³, M. M. Duras⁷⁶, J. M. Durham⁶², D. Dutta⁵⁷, A. Dziurda³⁵, A. Dzyuba³⁸, S. Easo⁵², U. Egede⁶⁴, A. Egorychev³⁸, V. Egorychev³⁸, C. Eirea Orro⁴¹, S. Eisenhardt⁵³, E. Ejopu⁵⁷, S. Ek-In⁴⁴, L. Eklund⁷⁷, M. E. Elashri⁶⁰, J. Ellbracht¹⁵, S. Ely⁵⁶, A. Ene³⁷, E. Eppe⁶⁰, S. Escher¹⁴, J. Eschle⁴⁵, S. Esen⁴⁵, T. Evans⁵⁷, F. Fabiano^{27,43,h}, L. N. Falcao¹, Y. Fan⁶, B. Fang^{11,69}, L. Fantini^{73,p}, M. Faria⁴⁴, K. Farmer⁵³, S. Farry⁵⁵, D. Fazzini^{26,m}, L. F. Felkowski⁷⁶, M. Feng^{4,6}, M. Feo⁴³, M. Fernandez Gomez⁴¹, A. D. Fernez⁶¹, F. Ferrari²⁰, L. Ferreira Lopes⁴⁴, F. Ferreira Rodrigues², S. Ferreres Sole³², M. Ferrillo⁴⁵, M. Ferro-Luzzi⁴³, S. Filippov³⁸, R. A. Fini¹⁹, M. Fiorini^{21,i}, M. Firlej³⁴, K. M. Fischer⁵⁸, D. S. Fitzgerald⁷⁸, C. Fitzpatrick⁵⁷, T. Fiutowski³⁴, F. Fleuret¹², M. Fontana²⁰, F. Fontanelli^{24,k}, L. F. Foreman⁵⁷, R. Forty⁴³, D. Foulds-Holt⁵⁰, V. Franco Lima⁵⁵, M. Franco Sevilla⁶¹, M. Frank⁴³, E. Franzoso^{21,i}, G. Frau¹⁷, C. Frei⁴³, D. A. Friday⁵⁷, L. F. Frontini^{25,1}, J. Fu⁶, Q. Fuehring¹⁵, T. Fulghesu¹³, E. Gabriel³², G. Galati^{19,f}, M. D. Galati³², A. Gallas Torreira⁴¹, D. Galli^{20,g}, S. Gambetta^{43,53}, M. Gandelman², P. Gandini²⁵, H. G. Gao⁶, R. Gao⁵⁸, Y. Gao⁷, Y. Gao⁵, M. Garau^{27,h}, L. M. Garcia Martin⁴⁴, P. Garcia Moreno⁴⁰, J. Garcia Pardiñas⁴³, B. Garcia Plana⁴¹, F. A. Garcia Rosales¹², L. Garrido⁴⁰, C. Gaspar⁴³, R. E. Geertsema³², L. L. Gerken¹⁵, E. Gersabeck⁵⁷, M. Gersabeck⁵⁷, T. Gershon⁵¹, L. Giambastiani²⁸, V. Gibson⁵⁰, H. K. Giemza³⁶, A. L. Gilman⁵⁸, M. Giovannetti²³, A. Gioventù⁴¹, P. Gironella Gironell⁴⁰, C. Giugliano^{21,i}, M. A. Giza³⁵, K. Gizdov⁵³, E. L. Gkougkousis⁴³, V. V. Gligorov¹³, C. Göbel⁶⁵, E. Golobardes³⁹, D. Golubkov³⁸, A. Golutvin^{38,43,56}, A. Gomes^{1,a}, S. Gomez Fernandez⁴⁰, F. Goncalves Abrantes⁵⁸, M. Goncerz³⁵, G. Gong³, J. A. Gooding¹⁵, I. V. Gorelov³⁸, C. Gotti²⁶, J. P. Grabowski⁷¹, L. A. Granado Cardoso⁴³, E. Graugés⁴⁰, E. Graverini⁴⁴, G. Graziani, A. T. Grecu³⁷, L. M. Greeven³², N. A. Grieser⁶⁰, L. Grillo⁵⁴, S. Gromov³⁸, C. Gu¹², M. Guarise^{21,i}, M. Guittiere¹¹, V. Guliaeva³⁸, P. A. Günther¹⁷, A. K. Guseinov³⁸, E. Gushchin³⁸, Y. Guz^{5,38,43}, T. Gys⁴³, T. Hadavizadeh⁶⁴, C. Hadjivasilou⁶¹, G. Haefeli⁴⁴, C. Haen⁴³, J. Haimberger⁴³, S. C. Haines⁵⁰, T. Halewood-leagas⁵⁵, M. M. Halvorsen⁴³, P. M. Hamilton⁶¹, J. Hammerich⁵⁵, Q. Han⁷, X. Han¹⁷, S. Hansmann-Menzemer¹⁷, L. Hao⁶, N. Harnew⁵⁸, T. Harrison⁵⁵, C. Hasse⁴³, M. Hatch⁴³, J. He^{6,c}, K. Heijhoff³², F. H. Hemmer⁴³, C. Henderson⁶⁰, R. D. L. Henderson^{51,64}, A. M. Hennequin⁴³, K. Hennessy⁵⁵, L. Henry⁴⁴, J. Herd⁵⁶, J. Heuel¹⁴, A. Hicheur², D. Hill⁴⁴, M. Hilton⁵⁷, S. E. Hollitt¹⁵, J. Horswill⁵⁷, R. Hou⁷, J. Hu¹⁷, J. Hu⁶⁷, W. Hu⁵, X. Hu³, W. Huang⁶, X. Huang⁶⁹, W. Hulsbergen³², R. J. Hunter⁵¹, M. Hushchyn³⁸, D. Hutchcroft⁵⁵, P. Ibis¹⁵, M. Idzik³⁴, D. Ilin³⁸, P. Ilten⁶⁰, A. Inglessi³⁸, A. Iniuikhin³⁸, A. Ishteev³⁸, K. Ivshin³⁸, R. Jacobsson⁴³, H. Jage¹⁴, S. J. Jaimes Elles^{42,70}, S. Jakobsen⁴³, E. Jans³², B. K. Jashal⁴², A. Jawahery⁶¹, V. Jevtic¹⁵, E. Jiang⁶¹, X. Jiang^{4,6}, Y. Jiang⁶, Y. J. Jiang⁵, M. John⁵⁸, D. Johnson⁵⁹, C. R. Jones⁵⁰, T. P. Jones⁵¹, S. J. Joshi³⁶, B. Jost⁴³, N. Jurik⁴³, I. Juszcak³⁵, D. Kaminaris⁴⁴, S. Kandybei⁴⁶, Y. Kang³, M. Karacson⁴³, D. Karpenkov³⁸, M. Karpov³⁸, J. W. Kautz⁶⁰, F. Keizer⁴³, D. M. Keller⁶³, M. Kenzie⁵¹, T. Ketel³², B. Khanji⁶³, A. Kharisova³⁸, S. Kholodenko³⁸, G. Khreich¹¹, T. Kim¹⁴, V. S. Kirsebom⁴⁴, O. Kitouni⁵⁹, S. Klaver³³, N. Kleijne^{29,q}, K. Klimaszewski³⁶, M. R. Kmiec³⁶, S. Koliev⁴⁷, L. Kolk¹⁵, A. Kondybayeva³⁸, A. Konoplyannikov³⁸, P. Kopciwicz³⁴, R. Kopečna¹⁷, P. Koppenburg³², M. Korolev³⁸, I. Kostiuik³², O. Kot⁴⁷, S. Kotriakhova, A. Kozachuk³⁸, P. Kravchenko³⁸, L. Kravchuk³⁸, M. Kreps⁵¹, S. Kretzschmar¹⁴, P. Krokovny³⁸, W. Krupa⁶³,

W. Krzemien³⁶, J. Kubat¹⁷, S. Kubis⁷⁶, W. Kucewicz³⁵, M. Kucharczyk³⁵, V. Kudryavtsev³⁸, E. K. Kulikova³⁸, A. Kupsc⁷⁷, D. Lacarrere⁴³, G. Lafferty⁵⁷, A. Lai²⁷, A. Lampis^{27,h}, D. Lancierini⁴⁵, C. Landesa Gomez⁴¹, J. J. Lane⁶⁴, R. Lane⁴⁹, C. Langenbruch¹⁷, J. Langer¹⁵, O. Lantwin³⁸, T. Latham⁵¹, F. Lazzari^{29,r}, C. Lazzeroni⁴⁸, R. Le Gac¹⁰, S. H. Lee⁷⁸, R. Lefèvre⁹, A. Leflat³⁸, S. Legotin³⁸, P. Lenisa^{21,i}, O. Leroy¹⁰, T. Lesiak³⁵, B. Leverington¹⁷, A. Li³, H. Li⁶⁷, K. Li⁷, L. Li⁵⁷, P. Li⁴³, P.-R. Li⁶⁸, S. Li⁷, T. Li⁴, T. Li⁶⁷, Y. Li⁴, Z. Li⁶³, Z. Lian³, X. Liang⁶³, C. Lin⁶, T. Lin⁵², R. Lindner⁴³, V. Lisovskyi⁴⁴, R. Litvinov^{27,h}, G. Liu⁶⁷, H. Liu⁶, K. Liu⁶⁸, Q. Liu⁶, S. Liu^{4,6}, A. Lobo Salvia⁴⁰, A. Loi²⁷, J. Lomba Castro⁴¹, I. Longstaff⁵⁴, J. H. Lopes², A. Lopez Huertas⁴⁰, S. L.ópez Soliño⁴¹, G. H. Lovell⁵⁰, Y. Lu^{4,b}, C. Lucarelli^{22,j}, D. Lucchesi^{28,o}, S. Luchuk³⁸, M. Lucio Martinez⁷⁵, V. Lukashenko^{32,47}, Y. Luo³, A. Lupato²⁸, E. Luppi^{21,i}, K. Lynch¹⁸, X.-R. Lyu⁶, R. Ma⁶, S. Maccolini¹⁵, F. Machefert¹¹, F. Maciuc³⁷, I. Mackay⁵⁸, V. Macko⁴⁴, L. R. Madhan Mohan⁵⁰, M. M. Madurai⁴⁸, A. Maevskiy³⁸, D. Maisuzenko³⁸, M. W. Majewski³⁴, J. J. Malczewski³⁵, S. Malde⁵⁸, B. Malecki^{35,43}, A. Malinin³⁸, T. Maltsev³⁸, G. Manca^{27,h}, G. Mancinelli¹⁰, C. Mancuso^{11,25,1}, R. Manera Escalero⁴⁰, D. Manuzzi²⁰, C. A. Manzari⁴⁵, D. Marangotto^{25,1}, J. F. Marchand⁸, U. Marconi²⁰, S. Mariani⁴³, C. Marin Benito⁴⁰, J. Marks¹⁷, A. M. Marshall⁴⁹, P. J. Marshall⁵⁵, G. Martelli^{73,p}, G. Martellotti³⁰, L. Martinazzoli^{43,m}, M. Martinelli^{26,m}, D. Martinez Santos⁴¹, F. Martinez Vidal⁴², A. Massafferri¹, M. Materok¹⁴, R. Matev⁴³, A. Mathad⁴⁵, V. Matiunin³⁸, C. Matteuzzi^{26,63}, K. R. Mattioli¹², A. Mauri⁵⁶, E. Maurice¹², J. Mauricio⁴⁰, M. Mazurek⁴³, M. McCann⁵⁶, L. Mcconnell¹⁸, T. H. McGrath⁵⁷, N. T. McHugh⁵⁴, A. McNab⁵⁷, R. McNulty¹⁸, B. Meadows⁶⁰, G. Meier¹⁵, D. Melnychuk³⁶, M. Merk^{32,75}, A. Merli²⁵, L. Meyer Garcia², D. Miao^{4,6}, H. Miao⁶, M. Mikhasenko^{71,d}, D. A. Milanes⁷⁰, M. Milovanovic⁴³, M.-N. Minard^{8,*}, A. Minotti^{26,m}, E. Minucci⁶³, T. Miralles⁹, S. E. Mitchell⁵³, B. Mitreska¹⁵, D. S. Mitzel¹⁵, A. Modak⁵², A. Mödden¹⁵, R. A. Mohammed⁵⁸, R. D. Moise¹⁴, S. Mokhnenko³⁸, T. Mombächer⁴¹, M. Monk^{51,64}, I. A. Monroy⁷⁰, S. Monteil⁹, G. Morello²³, M. J. Morello^{29,q}, M. P. Morgenthaler¹⁷, J. Moron³⁴, A. B. Morris⁴³, A. G. Morris¹⁰, R. Mountain⁶³, H. Mu³, Z. M. Mu⁵, E. Muhammad⁵¹, F. Muheim⁵³, M. Mulder⁷⁴, K. Müller⁴⁵, D. Murray⁵⁷, R. Murta⁵⁶, P. Muzzetto^{27,h}, P. Naik⁵⁵, T. Nakada⁴⁴, R. Nandakumar⁵², T. Nanut⁴³, I. Nasteva², M. Needham⁵³, N. Neri^{25,1}, S. Neubert⁷¹, N. Neufeld⁴³, P. Neustroev³⁸, R. Newcombe⁵⁶, J. Nicolini^{11,15}, D. Nicotra⁷⁵, E. M. Niel⁴⁴, S. Nieswand¹⁴, N. Nikitin³⁸, N. S. Nolte⁵⁹, C. Normand^{8,27,h}, J. Novoa Fernandez⁴¹, G. N. Nowak⁶⁰, C. Nunez⁷⁸, A. Oblakowska-Mucha³⁴, V. Obraztsov³⁸, T. Oeser¹⁴, S. Okamura^{21,43,i}, R. Oldeman^{27,h}, F. Oliva⁵³, M. O. Olocco¹⁵, C. J. G. Onderwater⁷⁵, R. H. O'Neil⁵³, J. M. Otorola Goicochea², T. Ovsianikova³⁸, P. Owen⁴⁵, A. Oyanguren⁴², O. Ozcelik⁵³, K. O. Padeken⁷¹, B. Pagare⁵¹, P. R. Pais¹⁷, T. Pajero⁵⁸, A. Palano¹⁹, M. Palutan²³, G. Panshin³⁸, L. Paolucci⁵¹, A. Papanestis⁵², M. Pappagallo^{19,f}, L. L. Pappalardo^{21,i}, C. Pappenheimer⁶⁰, C. Parkes⁵⁷, B. Passalacqua²¹, G. Passaleva²², A. Pastore¹⁹, M. Patel⁵⁶, C. Patrignani^{20,g}, C. J. Pawley⁷⁵, A. Pellegrino³², M. Pepe Altarelli²³, S. Perazzini²⁰, D. Pereima³⁸, A. Pereiro Castro⁴¹, P. Perret⁹, A. Perro⁴³, K. Petridis⁴⁹, A. Petrolini^{24,k}, S. Petrucci⁵³, M. Petruzzo²⁵, H. Pham⁶³, A. Philippov³⁸, L. Pica^{29,q}, M. Piccini⁷³, B. Pietrzyk⁸, G. Pietrzyk¹¹, D. Pinci³⁰, F. Pisani⁴³, M. Pizzichemi^{26,m}, V. Placinta³⁷, J. Plews⁴⁸, M. Plo Casasus⁴¹, F. Polci^{13,43}, M. Poli Lener²³, A. Poluektov¹⁰, N. Polukhina³⁸, I. Polyakov⁴³, E. Polycarpo², S. Ponce⁴³, D. Popov^{6,43}, S. Poslavskii³⁸, K. Prasanth³⁵, L. Promberger¹⁷, C. Prouve⁴¹, V. Pugatch⁴⁷, V. Puill¹¹, G. Punzi^{29,r}, H. R. Qi³, W. Qian⁶, N. Qin³, S. Qu³, R. Quagliani⁴⁴, B. Rachwal³⁴, J. H. Rademacker⁴⁹, R. Rajagopalan⁶³, M. Rama²⁹, M. Ramos Pernas⁵¹, M. S. Rangel², F. Ratnikov³⁸, G. Raven³³, M. Rebollo De Miguel⁴², F. Redi⁴³, J. Reich⁴⁹, F. Reiss⁵⁷, Z. Ren³, P. K. Resmi⁵⁸, R. Ribatti^{29,q}, S. Ricciardi⁵², K. Richardson⁵⁹, M. Richardson-Slipper⁵³, K. Rinnert⁵⁵, P. Robbe¹¹, G. Robertson⁵³, E. Rodrigues^{43,55}, E. Rodriguez Fernandez⁴¹, J. A. Rodriguez Lopez⁷⁰, E. Rodriguez Rodriguez⁴¹, D. L. Rolf⁴³, A. Rollings⁵⁸, P. Roloff⁴³, V. Romanovskiy³⁸, M. Romero Lamas⁴¹, A. Romero Vidal⁴¹, F. Ronchetti⁴⁴, M. Rotondo²³, M. S. Rudolph⁶³, T. Ruf⁴³, R. A. Ruiz Fernandez⁴¹, J. Ruiz Vidal⁴², A. Ryzhikov³⁸, J. Ryzka³⁴, J. J. Saborido Silva⁴¹, N. Sagidova³⁸, N. Sahoo⁴⁸, B. Saitta^{27,h}, M. Salomoni⁴³, C. Sanchez Gras³², I. Sanderswood⁴², R. Santacesaria³⁰, C. Santamarina Rios⁴¹, M. Santimaria²³, L. Santoro¹, E. Santovetti³¹, D. Saranin³⁸, G. Sarpis⁵³, M. Sarpis⁷¹, A. Sarti³⁰, C. Satriano^{30,s}, A. Satta³¹, M. Saur⁵, D. Savrina³⁸, H. Sazak⁹, L. G. Scantlebury Smead⁵⁸, A. Scarabotto¹³, S. Schael¹⁴, S. Scherl⁵⁵, A. M. Schertz⁷², M. Schiller⁵⁴, H. Schindler⁴³, M. Schmelling¹⁶, B. Schmidt⁴³, S. Schmitt¹⁴, O. Schneider⁴⁴, A. Schopper⁴³, M. Schubiger³², N. Schulte¹⁵, S. Schulte⁴⁴, M. H. Schune¹¹, R. Schwemmer⁴³, G. Schwering¹⁴, B. Sciascia²³, A. Sciucati⁴³, S. Sellam⁴¹, A. Semennikov³⁸, M. Senghi Soares³³, A. Sergi^{24,k}, N. Serra^{43,45}, L. Sestini²⁸, A. Seuthe¹⁵, Y. Shang⁵, D. M. Shangase⁷⁸,

M. Shapkin³⁸, I. Shchemerov³⁸, L. Shchutska⁴⁴, T. Shears⁵⁵, L. Shekhtman³⁸, Z. Shen⁵, S. Sheng^{4,6}, S. S. Sheth⁴³, V. Shevchenko³⁸, B. Shi⁶, E. B. Shields^{26,m}, Y. Shimizu¹¹, E. Shmanin³⁸, R. Shorkin³⁸, J. D. Shupperd⁶³, B. G. Siddi^{21,i}, R. Silva Coutinho⁶³, G. Simi²⁸, S. Simone^{19,f}, M. Singla⁶⁴, N. Skidmore⁵⁷, R. Skuza¹⁷, T. Skwarnicki⁶³, M. W. Slater⁴⁸, J. C. Smallwood⁵⁸, J. G. Smeaton⁵⁰, E. Smith⁴⁵, K. Smith⁶², M. Smith⁵⁶, A. Snoch³², L. Soares Lavra⁵³, M. D. Sokoloff⁶⁰, F. J. P. Soler⁵⁴, A. Solomin^{38,49}, A. Solovov³⁸, I. Solovyev³⁸, R. Song⁶⁴, Y. Song³, Y. S. Song⁵, Y. S. Song⁴⁴, F. L. Souza De Almeida², B. Souza De Paula², E. Spadaro Norella^{25,1}, E. Spedicato²⁰, J. G. Speer¹⁵, E. Spiridenkov³⁸, P. Spradlin⁵⁴, V. Sriskaran⁴³, F. Stagni⁴³, M. Stahl⁴³, S. Stahl⁴³, S. Stanislaus⁵⁸, E. N. Stein⁴³, O. Steinkamp⁴⁵, O. Stenyakin³⁸, H. Stevens¹⁵, D. Strelakina³⁸, Y. S. Su⁶, F. Suljik⁵⁸, J. Sun²⁷, L. Sun⁶⁹, Y. Sun⁶¹, P. N. Swallow⁴⁸, K. Swientek³⁴, A. Szabelski³⁶, T. Szumlak³⁴, M. Szymanski⁴³, Y. Tan³, S. Taneja⁵⁷, M. D. Tat⁵⁸, A. Terentev⁴⁵, F. Teubert⁴³, E. Thomas⁴³, D. J. D. Thompson⁴⁸, H. Tilquin⁵⁶, V. Tisserand⁹, S. T'Jampens⁸, M. Tobin⁴, L. Tomassetti^{21,i}, G. Tonani^{25,1}, X. Tong⁵, D. Torres Machado¹, L. Toscano¹⁵, D. Y. Tou³, C. Trippel⁴⁴, G. Tuci¹⁷, N. Tuning³², A. Ukleja³⁶, D. J. Unverzagt¹⁷, E. Ursov³⁸, A. Usachov³³, A. Ustyuzhanin³⁸, U. Uwer¹⁷, V. Vagnoni²⁰, A. Valassi⁴³, G. Valenti²⁰, N. Valls Canudas³⁹, M. Van Dijk⁴⁴, H. Van Hecke⁶², E. van Herwijnen⁵⁶, C. B. Van Hulse^{41,v}, R. Van Laak⁴⁴, M. van Veghel³², R. Vazquez Gomez⁴⁰, P. Vazquez Regueiro⁴¹, C. Vázquez Sierra⁴¹, S. Vecchi²¹, J. J. Velthuis⁴⁹, M. Veltri^{22,u}, A. Venkateswaran⁴⁴, M. Vesterinen⁵¹, D. Vieira⁶⁰, M. Vieites Diaz⁴⁴, X. Vilasis-Cardona³⁹, E. Vilella Figueras⁵⁵, A. Villa²⁰, P. Vincent¹³, F. C. Volle¹¹, D. vom Bruch¹⁰, V. Vorobyev³⁸, N. Voropaev³⁸, K. Vos⁷⁵, C. Vrahas⁵³, J. Walsh²⁹, E. J. Walton⁶⁴, G. Wan⁵, C. Wang¹⁷, G. Wang⁷, J. Wang⁵, J. Wang⁴, J. Wang³, J. Wang⁶⁹, M. Wang²⁵, N. W. Wang⁶, R. Wang⁴⁹, X. Wang⁶⁷, Y. Wang⁷, Z. Wang⁴⁵, Z. Wang³, Z. Wang⁶, J. A. Ward^{51,64}, N. K. Watson⁴⁸, D. Websdale⁵⁶, Y. Wei⁵, B. D. C. Westhenry⁴⁹, D. J. White⁵⁷, M. Whitehead⁵⁴, A. R. Wiederhold⁵¹, D. Wiedner¹⁵, G. Wilkinson⁵⁸, M. K. Wilkinson⁶⁰, I. Williams⁵⁰, M. Williams⁵⁹, M. R. J. Williams⁵³, R. Williams⁵⁰, F. F. Wilson⁵², W. Wislicki³⁶, M. Witek³⁵, L. Witola¹⁷, C. P. Wong⁶², G. Wormser¹¹, S. A. Wotton⁵⁰, H. Wu⁶³, J. Wu⁷, Y. Wu⁵, K. Wyllie⁴³, S. Xian⁶⁷, Z. Xiang⁶, Y. Xie⁷, A. Xu²⁹, J. Xu⁶, L. Xu³, L. Xu³, M. Xu⁵¹, Z. Xu⁹, Z. Xu⁶, Z. Xu⁴, D. Yang³, S. Yang⁶, X. Yang⁵, Y. Yang²⁴, Z. Yang⁵, Z. Yang⁶¹, V. Yeroshenko¹¹, H. Yeung⁵⁷, H. Yin⁷, C. Y. Yu⁵, J. Yu⁶⁶, X. Yuan⁴, E. Zaffaroni⁴⁴, M. Zavertyaev¹⁶, M. Zdybal³⁵, M. Zeng³, C. Zhang⁵, D. Zhang⁷, J. Zhang⁶, L. Zhang³, S. Zhang⁶⁶, S. Zhang⁵, Y. Zhang⁵, Y. Zhang⁵⁸, Y. Zhao¹⁷, A. Zharkova³⁸, A. Zhelezov¹⁷, Y. Zheng⁶, T. Zhou⁵, X. Zhou⁷, Y. Zhou⁶, V. Zhovkovska¹¹, L. Z. Zhu⁶, X. Zhu³, X. Zhu⁷, Z. Zhu⁶, V. Zhukov^{14,38}, J. Zhuo⁴², Q. Zou^{4,6}, S. Zucchelli^{20,g}, D. Zuliani²⁸, G. Zunica⁵⁷

¹ Centro Brasileiro de Pesquisas Físicas (CBPF), Rio de Janeiro, Brazil

² Universidade Federal do Rio de Janeiro (UFRJ), Rio de Janeiro, Brazil

³ Center for High Energy Physics, Tsinghua University, Beijing, China

⁴ Institute Of High Energy Physics (IHEP), Beijing, China

⁵ School of Physics State Key Laboratory of Nuclear Physics and Technology, Peking University, Beijing, China

⁶ University of Chinese Academy of Sciences, Beijing, China

⁷ Institute of Particle Physics, Central China Normal University, Wuhan, Hubei, China

⁸ Université Savoie Mont Blanc, CNRS, IN2P3-LAPP, Annecy, France

⁹ Université Clermont Auvergne, CNRS/IN2P3, LPC, Clermont-Ferrand, France

¹⁰ Aix Marseille Univ, CNRS/IN2P3, CPPM, Marseille, France

¹¹ Université Paris-Saclay, CNRS/IN2P3, IJCLab, Orsay, France

¹² Laboratoire Leprince-Ringuet, CNRS/IN2P3, Ecole Polytechnique, Institut Polytechnique de Paris, Palaiseau, France

¹³ LPNHE, Sorbonne Université, Paris Diderot Sorbonne Paris Cité, CNRS/IN2P3, Paris, France

¹⁴ I. Physikalisches Institut, RWTH Aachen University, Aachen, Germany

¹⁵ Fakultät Physik, Technische Universität Dortmund, Dortmund, Germany

¹⁶ Max-Planck-Institut für Kernphysik (MPIK), Heidelberg, Germany

¹⁷ Physikalisches Institut, Ruprecht-Karls-Universität Heidelberg, Heidelberg, Germany

¹⁸ School of Physics, University College Dublin, Dublin, Ireland

¹⁹ INFN Sezione di Bari, Bari, Italy

²⁰ INFN Sezione di Bologna, Bologna, Italy

²¹ INFN Sezione di Ferrara, Ferrara, Italy

- 22 INFN Sezione di Firenze, Florence, Italy
- 23 INFN Laboratori Nazionali di Frascati, Frascati, Italy
- 24 INFN Sezione di Genova, Genoa, Italy
- 25 INFN Sezione di Milano, Milan, Italy
- 26 INFN Sezione di Milano-Bicocca, Milan, Italy
- 27 INFN Sezione di Cagliari, Monserrato, Italy
- 28 Università degli Studi di Padova, Università e INFN, Padua, Italy
- 29 INFN Sezione di Pisa, Pisa, Italy
- 30 INFN Sezione di Roma La Sapienza, Rome, Italy
- 31 INFN Sezione di Roma Tor Vergata, Rome, Italy
- 32 Nikhef National Institute for Subatomic Physics, Amsterdam, The Netherlands
- 33 Nikhef National Institute for Subatomic Physics and VU University Amsterdam, Amsterdam, The Netherlands
- 34 AGH-University of Science and Technology, Faculty of Physics and Applied Computer Science, Kraków, Poland
- 35 Henryk Niewodniczanski Institute of Nuclear Physics Polish Academy of Sciences, Kraków, Poland
- 36 National Center for Nuclear Research (NCBJ), Warsaw, Poland
- 37 Horia Hulubei National Institute of Physics and Nuclear Engineering, Bucharest-Magurele, Romania
- 38 Affiliated with an Institute Covered by a Cooperation Agreement with CERN, Geneva, Switzerland
- 39 DS4DS, La Salle, Universitat Ramon Llull, Barcelona, Spain
- 40 ICCUB, Universitat de Barcelona, Barcelona, Spain
- 41 Instituto Galego de Física de Altas Enerxías (IGFAE), Universidade de Santiago de Compostela, Santiago de Compostela, Spain
- 42 Instituto de Física Corpuscular, Centro Mixto Universidad de Valencia-CSIC, Valencia, Spain
- 43 European Organization for Nuclear Research (CERN), Geneva, Switzerland
- 44 Institute of Physics, Ecole Polytechnique Fédérale de Lausanne (EPFL), Lausanne, Switzerland
- 45 Physik-Institut, Universität Zürich, Zürich, Switzerland
- 46 NSC Kharkiv Institute of Physics and Technology (NSC KIPT), Kharkiv, Ukraine
- 47 Institute for Nuclear Research of the National Academy of Sciences (KINR), Kyiv, Ukraine
- 48 University of Birmingham, Birmingham, UK
- 49 H.H. Wills Physics Laboratory, University of Bristol, Bristol, UK
- 50 Cavendish Laboratory, University of Cambridge, Cambridge, UK
- 51 Department of Physics, University of Warwick, Coventry, UK
- 52 STFC Rutherford Appleton Laboratory, Didcot, UK
- 53 School of Physics and Astronomy, University of Edinburgh, Edinburgh, UK
- 54 School of Physics and Astronomy, University of Glasgow, Glasgow, UK
- 55 Oliver Lodge Laboratory, University of Liverpool, Liverpool, UK
- 56 Imperial College London, London, UK
- 57 Department of Physics and Astronomy, University of Manchester, Manchester, UK
- 58 Department of Physics, University of Oxford, Oxford, UK
- 59 Massachusetts Institute of Technology, Cambridge, MA, USA
- 60 University of Cincinnati, Cincinnati, OH, USA
- 61 University of Maryland, College Park, MD, USA
- 62 Los Alamos National Laboratory (LANL), Los Alamos, NM, USA
- 63 Syracuse University, Syracuse, NY, USA
- 64 School of Physics and Astronomy, Monash University, Melbourne, Australia, associated to ⁵¹
- 65 Pontifícia Universidade Católica do Rio de Janeiro (PUC-Rio), Rio de Janeiro, Brazil, associated to ²
- 66 Physics and Micro Electronic College, Hunan University, Changsha, China, associated to ⁷
- 67 Guangdong Provincial Key Laboratory of Nuclear Science, Guangdong-Hong Kong Joint Laboratory of Quantum Matter, Institute of Quantum Matter, South China Normal University, Guangzhou, China, associated to ³
- 68 Lanzhou University, Lanzhou, China, associated to ⁴
- 69 School of Physics and Technology, Wuhan University, Wuhan, China, associated to ³
- 70 Departamento de Física, Universidad Nacional de Colombia, Bogota, Colombia, associated to ¹³
- 71 Universität Bonn-Helmholtz-Institut für Strahlen und Kernphysik, Bonn, Germany, associated to ¹⁷
- 72 Eotvos Lorand University, Budapest, Hungary, associated to ⁴³

- ⁷³ INFN Sezione di Perugia, Perugia, Italy, associated to ²¹
- ⁷⁴ Van Swinderen Institute, University of Groningen, Groningen, The Netherlands, associated to ³²
- ⁷⁵ Universiteit Maastricht, Maastricht, The Netherlands, associated to ³²
- ⁷⁶ Tadeusz Kosciuszko Cracow University of Technology, Kraków, Poland, associated to ³⁵
- ⁷⁷ Department of Physics and Astronomy, Uppsala University, Uppsala, Sweden, associated to ⁵⁴
- ⁷⁸ University of Michigan, Ann Arbor, MI, USA, associated to ⁶³
- ^a Universidade de Brasília, Brasília, Brazil
- ^b Central South University, Changsha, China
- ^c Hangzhou Institute for Advanced Study, UCAS, Hangzhou, China
- ^d Excellence Cluster ORIGINS, Munich, Germany
- ^e Universidad Nacional Autónoma de Honduras, Tegucigalpa, Honduras
- ^f Università di Bari, Bari, Italy
- ^g Università di Bologna, Bologna, Italy
- ^h Università di Cagliari, Cagliari, Italy
- ⁱ Università di Ferrara, Ferrara, Italy
- ^j Università di Firenze, Florence, Italy
- ^k Università di Genova, Genoa, Italy
- ^l Università degli Studi di Milano, Milan, Italy
- ^m Università di Milano Bicocca, Milan, Italy
- ⁿ Università di Modena e Reggio Emilia, Modena, Italy
- ^o Università di Padova, Padua, Italy
- ^p Università di Perugia, Perugia, Italy
- ^q Scuola Normale Superiore, Pisa, Italy
- ^r Università di Pisa, Pisa, Italy
- ^s Università della Basilicata, Potenza, Italy
- ^t Università di Roma Tor Vergata, Rome, Italy
- ^u Università di Urbino, Urbino, Italy
- ^v Universidad de Alcalá, Alcalá de Henares, Spain
- ^w Universidade da Coruña, Coruña, Spain
- *Deceased